Title: Multisite imaging of neural activity using a genetically encoded calcium sensor in the honey bee

Short title: Neural recordings using transgenic honey bees

Authors: Julie Carcaud[1*], Marianne Otte[2], Bernd Grünewald[3], Albrecht Haase[4,5,6], Jean-Christophe Sandoz[1,6], Martin Beye[2,6]

*Corresponding author: Julie Carcaud, Evolution, Genomes, Behavior and Ecology, Université Paris-Saclay, CNRS, IRD, Gif-sur-Yvette, France. Email: julie.carcaud@universite-paris-saclay.fr. Phone: +33169154973

Author's addresses:

[1] Evolution, Genomes, Behavior and Ecology, Université Paris-Saclay, CNRS, IRD, Gif-sur-Yvette, France

[2] Evolutionnary Genetics, Heinrich Heine University Düsseldorf, Düsseldorf, Germany

[3]Institut für Bienenkunde, Polytechnische Gesellschaft, FB Biowissenschaften, Goethe-University, Frankfurt am Main, Germany

[4] Center for Mind/Brain Sciences (CIMeC), University of Trento, Rovereto, Italy

[5] Department of Physics, University of Trento, Trento, Italy

[6] These authors jointly supervised this work

ABSTRACT

Understanding of the neural bases for complex behaviors in Hymenoptera insect species has been limited by a lack of tools that allow measuring neuronal activity simultaneously in different brain regions. Here, we developed the first pan-neuronal genetic driver in a Hymenopteran model organism, the honey bee, and expressed the calcium indicator GCaMP6f under the control of the honey bee *synapsin* promoter. We show that GCaMP6f is widely expressed in the honey bee brain, allowing to record neural activity from multiple brain regions. To assess the power of this tool, we focused on the olfactory system, recording simultaneous responses from the antennal lobe, and from the more poorly investigated lateral horn and mushroom body calyces. Neural responses to 16 distinct odorants demonstrate that odorant quality (chemical structure) and quantity are faithfully encoded in the honey bee antennal lobe. In contrast, odor coding in the lateral horn departs from this simple physico-chemical coding, supporting the role of this structure in coding the biological value of odorants. We further demonstrate robust neural responses to several bee pheromone odorants, key drivers of social behavior, in the lateral horn. Combined, these brain recordings represent the first use of a neurogenetic tool for recording large-scale neural activity in a eusocial insect, and will be of utility in assessing the neural underpinnings of olfactory and other sensory modalities and of social behaviors and cognitive abilities.

Keywords: Insect, honey bee, brain, olfaction, transgenesis, calcium imaging, GCaMP

52 **INTRODUCTION**

53

54 Sociality is classified as one of the major transitions in evolution, and animals often form social
55 groups because the benefits of grouping (either direct or indirect) outweigh the costs of breeding
56 independently [1, 2]. The most advanced level of sociality is found in eusocial insect societies [3, 4],
57 and the insect order Hymenoptera (including ants, bees, and wasps) presents the largest number of
58 eusocial species. Among them, honey bees are a classical model for the study of eusocial behavior, as
59 they live in colonies composed of up to 60,000 individuals, consisting of three adult castes (queen,
60 worker, and male). Within the worker caste, honey bees show a clear division of labor with a
61 specialization of roles [5]. The success of honey bee colonies lies in the capacity of all members of the
62 society to behave in a well-organized and context-dependent manner, a social behavior mediated in
63 part by olfactory cues such as pheromones used for communication within the colony [6].

64 Previous research found that this sophisticated social behavior is associated with higher
65 cognitive abilities in these insects, and in this context, honey bees are a mainstream model for studying
66 higher-order insect cognition such as navigation [7], rule learning [8], social learning [9], dance
67 communication [10], but also olfactory perception and learning [11-13]. However, whether the
68 evolutionary rise of these sophisticated social behaviors is associated with the formation of specific
69 neuronal pathways and structures has not been sufficiently resolved [14, 15]. Progress in
70 understanding these sophisticated behaviors and how social cues are processed and integrated with
71 higher-order cognitive abilities have in part been limited due to the lack of tools allowing to measure
72 neuronal activity simultaneously in different regions of the honey bee brain.

73 For now, honey bee neuroscience remains limited to the use of conventional neuroanatomy
74 [16], pharmacology [17], electrophysiology [18], and imaging tools [13, 19]. However, the development
75 of neurogenetic tools during the 20th century has provided unprecedented progress in our
76 understanding of the neural basis of behavior in other model species. Among others, this approach
77 allowed to decipher the brain circuits underlying aggressive behavior [20], courtship [21], or memory

78 [22] in a limited set of model species, both vertebrates such as mouse or zebrafish and invertebrates.
79 In insects, the fruit fly *Drosophila melanogaster* has been for many years the leading model for
80 investigating the neural basis of behavior, from gene expression to neural circuits [23-25]. Recently,
81 neurogenetic approaches have been developed in other Diptera such as mosquitoes [26, 27] and in
82 some Lepidoptera [28, 29] to understand specific behaviors such as human-host seeking [30, 31] or
83 insect-plant interactions [32], mainly focusing on their olfactory capabilities. However, genetic
84 methods are particularly difficult to apply in eusocial insects, since genetic transformation rates are
85 low, endogenous promoters for neuronal expressions are unknown and the genetically manipulated,
86 reproductive individuals (the queens) have to be maintained in larger colonies with workers in
87 containments [33].

88 Despite the difficulty, the recent use of the genome editing tool CRISPR/Cas9 in the honey bee
89 allowed to knock out specific genes, such as the sex-determining *dsx* gene [34], the olfactory co-
90 receptor gene *orco* [35], the gustatory receptor *AmGr3* gene [36], or the *Amyellow-y* gene [37]. Even
91 if these studies evaluated the effect of specific mutations at the neuronal [35] or the behavioral levels
92 [36], versatile genetic tools allowing to investigate the neural basis of a wide range of higher-order
93 social behaviors and learning in honey bees are still missing. The advent of genetically-encoded neural
94 activity sensors, in particular calcium sensors, has represented a major breakthrough in *Drosophila* or
95 mouse research [38-40], but such a critical tool for circuit dissection is still lacking in Hymenoptera.

96 To this aim, we developed the first pan-neuronal genetic driver in a Hymenopteran model
97 organism, the honey bee, and expressed the calcium indicator GCaMP6f under the control of the honey
98 bee *synapsin* promoter. We characterized its expression pattern in the honey bee brain and evaluated
99 its potential as a functional tool by recording neural activity upon olfactory stimulation. We show that
100 GCaMP6f expression allows to record olfactory responses from multiple brain regions, after simply
101 opening the brain capsule. By using a controlled panel of well-characterized odorants, we show that
102 the recorded signals reveal robust odor coding rules. This new pan-neuronal genetic driver also permits
103 to record neural activity from poorly recorded regions of the brain such as the lateral horn and the

104 mushroom body calyces, and allowed to find that olfactory chemical features are less represented in
105 the lateral horn than in the antennal lobe. This study opens new possibilities for neuroethological
106 research in the honey bee to study the neural basis of advanced social behaviors and cognitive skills.
107
108
109 **RESULTS**
110 This work aimed at expressing the calcium-sensitive protein GCaMP6f in a pan-neuronal manner in the
111 honey bee brain to record neural activity in this social insect.
112
113 **Generation of transgenic honey bees**
114 In order to generate a bee with a possibly pan-neuronally expressed calcium sensor, we introduced a
115 synapsin (syn) promoter GCaMP6f expression cassette (*syn-GCaMP6f*) into the genome using the
116 *PiggyBac* transposon system [33]. To generate this *syn-GCaMP6f* expression cassette we cloned the 1
117 kb promoter region together with the entire 5' untranslated region (5' UTR) of the *synapsin* gene from
118 the honey bee (S1 Fig), which we then fused with the coding sequence of the GCaMP6f sensor protein
119 (Fig 1A). We obtained transgenic *syn-GCaMP6f* queens using previously published procedures and a
120 hyperactive transposase [33, 41]. We instrumentally inseminated the queens and reared from only
121 one F0 queen the offspring 2nd generation queens (F1). Only 1% of those F1 queens were carrying the
122 transgene, which we identified from transgene amplifications. The 2nd generation *syn-GCaMP6f*
123 queens produced 50% *syn-GCaMP6f* worker offspring bees, which we used in the following
124 neuroanatomy and imaging experiments.
125
126 **Pattern expression of the GCaMP6f in the brain**
127 We first studied the pattern expression of GCaMP6f in the brain using immunostaining against
128 GFP (Fig 1B-D; S2 Fig), the green fluorescent protein which the GCaMP6f sensor contains. We found
129 clear and widespread staining throughout the brain, with strong staining in the antennal lobes (ALs),

130 the optic lobes (OLs), and the mushroom bodies (MBs), suggesting that the GCaMP6f protein is
131 ubiquitously expressed in all major brain structures. In comparison, wild type (WT) bees which do not
132 express the GCaMP6f protein show no staining throughout the brain (S2C Fig).

133 Within neurons of the transgenic bees expressing GCaMP6f, we found evidence of staining in
134 somata (Fig 1B left, S2A-B Fig; white arrows), neuronal processes (see for instance neural tracts around
135 the α-lobe; Fig 1B left, white arrows) as well as dendrites and terminal projections. At the level of the
136 AL (Fig 1C; S2 Fig), lateral and medial clusters of projection neurons and local interneurons somata
137 show strong GCaMP6f immunostaining. In addition, glomeruli seem homogeneously stained: staining
138 in the cortex suggests expression in olfactory sensory neurons (OSNs) terminal projections, whereas
139 staining in the glomerulus core suggests expression in projection neurons (PNs) dendrites and possibly
140 local neurons. Finally, the clearest expression of GCaMP6f was found in somata at the level of the
141 calyces of the MB (Fig 1D; S2B Fig). In these structures, different neuron types are stained, with somata
142 of class I Kenyon Cells in the cup-shaped calyces and class II Kenyon Cell somata lying outside the
143 calyces (see white arrow in Fig 1D; S2B Fig) [42, 43]. These staining patterns were similar in the
144 different bees we used for the immunostaining (S2A-B Fig). We found very broad expression in some
145 groups of neurons like the somata of antennal lobe neurons (Example shown in S3A Fig for a somata
146 cluster of local/projection neurons in caudo-lateral position) and at the same time heterogeneous
147 staining at the level of the Kenyon cells within MB calyces. We also found expression of GCaMP6f in
148 neurons outside of the central brain, for example in the photoreceptors of the ocelli (S3B Fig).

149 We next asked whether the cloned synapsin promoter used for GCaMP6f expression drives the
150 same expression pattern as the one of the *synapsin* gene. To answer this question, we performed a
151 complementary immunostaining targeting the synapsin protein (Fig 1B right, anti-SYNORF1 in red). We
152 found co-localized staining of GCaMP6f and synapsin within AL glomeruli both in the cortex and the
153 core (Fig 1C right), demonstrating co-expression within AL neurons. This experiment also shows
154 differences between GCaMP6f and synapsin stainings. The synapsin immunostaining allows to clearly
155 visualize presynaptic zones, for instance in AL glomeruli or microglomeruli in the MB calyces, but is not

156 present in the somata unlike GCaMP6f (Fig 1D, white arrows). This result indicates that even if
157 GCaMP6f is expressed in cells expressing synapsin (in theory all neurons), these 2 proteins appear to
158 be partially differently localized within neurons.

159 We conclude that GCaMP6f was widely expressed in the honey bee brain, one of the
160 prerequisites for whole-brain functional recordings of neural activity.

161

162 **Calcium imaging**

163 *Neural recordings in the whole brain*

164 GCaMP6f expression in neurons was then used to record neural activity in the honey bee brain (Fig 2).
165 As a proof of concept for the use of these bees in neuroethological research, we decided to focus here
166 on olfactory information processing, as olfaction is the best-understood sensory modality in honey
167 bees. Right after placing the bee in a recording chamber and opening its head capsule, we first
168 presented a few standard odorants while recording the whole brain surface accessible under the
169 microscope objective. Odorant presentations triggered a clear GCaMP fluorescence change from
170 several brain regions (Fig 2A), including the primary olfactory centers (the antennal lobes, ALs) and
171 both higher-order centers (the lateral horns, LHs and the mushroom bodies, MBs), known for their role
172 in olfactory processing. The use of GCaMP-expressing bees allowed us to record neural activity
173 simultaneously in all these structures (Fig 2B), while the presentation of an unscented air control did
174 not induce strong activity. Response amplitudes were stronger in the AL (Fig 2C left) than in the LH (Fig
175 2C middle) or in the MB (Fig 2C right). In all regions, the recorded calcium signals showed a biphasic
176 response, with a fluorescence increase upon odor presentation followed by a long undershoot. Such
177 biphasic signals are reminiscent of calcium signals previously recorded using bath-applied calcium-
178 sensitive dyes [44, 45]. This experiment represents the first recording of neural activity using
179 neurogenetic tools outside of Diptera.

180

181 *Neural recordings in the antennal lobe (AL)*

182 We then asked if the signals recorded using this genetically-encoded calcium sensor represent
183 neural signals that are meaningful in terms of sensory coding, focusing first on the primary olfactory
184 center, the antennal lobe (AL), since olfactory coding was best studied in this structure. To this aim,
185 we presented 16 aliphatic odorants used in previous imaging studies either after bath-application of a
186 cell-permeant calcium-sensitive dye (Calcium-green 2-AM, OSN recordings) [45] or after insertion of a
187 migrating calcium-sensitive dye within a neural tract (Fura-2 dextran, PN recordings) [19]. The
188 response patterns to the 16 aliphatic odors differed systematically according to their functional group
189 (primary or secondary alcohols, aldehydes, or ketones) or their carbon chain length (from 6 to 9
190 carbons) (Fig 3A). As observed with other calcium reporters, the presentation of each odorant induced
191 a biphasic signal in a different set of AL glomeruli while presentation of the air control or no stimulation
192 did not induce such response (Fig 3B, S4A Fig; S5 Data; S9 Data). Moreover, WT bees did not show any
193 signal in response to odor presentation (S4B Fig). The averaged AL response amplitudes were
194 significantly different from the air control for all 16 odors (Fig 3C; S1 Data; n = 11 honey bees, RM-
195 ANOVA, odor effect $F_{16,160}$ = 12.49, p = 8e-21, post hoc Dunnett tests p < 0.0097). Signal amplitudes
196 differed according to the odor (odor effect, p = 8e-21), and were related to the quantity of molecules
197 in headspace, since odor-evoked responses were highly correlated with the vapor pressure of the
198 odorants (Fig 3D, n = 11 honey bees, R^2 = 0.84, Fisher test $F_{1,14}$ = 73.72, p = 6e-7). Such a correlation
199 was also found in previous studies recording at AL input (OSNs) [45] or output (PNs) [19]. This strong
200 dependence explains why odor-evoked intensities recorded using genetically encoded GCaMP6f in this
201 study are highly correlated with odor-evoked intensities recorded in OSNs (S5A Fig, R^2 = 0.84, $F_{1,14}$ =
202 74.23, p = 6e-7) or in PNs (S5B Fig, R^2 = 0.78, $F_{1,14}$ = 49.73, p = 6e-6).

203 We then evaluated odor coding in the GCaMP bees by comparing similarity relationships
204 among odorants, by calculating Euclidian distances between response maps obtained for the different
205 odor pairs (S1 Data). First, we confirmed that within each bee, each odorant evokes a specific activity
206 pattern, as distances were lower for different presentations of the same odorant than for the
207 presentation of different odorants (Fig 3E, n = 11 honey bees, paired t-test t = 6.15, p = 1.08e-4). This

208 result fits with previous calcium imaging data both at AL input and output [46, 47]. We then performed
209 a hierarchical cluster analysis using Euclidian distances between odorants. We found a first segregation
210 between odorants with long chain lengths and odorants with short chain lengths (Fig 3F, C6-C7 vs. C8-
211 C9). Within the shorter chain length group, a further separation between functional groups appeared
212 based on the oxygen moiety (C=O for aldehydes and ketones vs. C-OH for alcohols). Within the longer
213 chain length group, aldehydes were separated from the other odorants. This analysis shows a clear
214 coding depending on the chemical structure of the odorants, and with remarkably similar results as in
215 previous studies using non-transgenic approaches [19, 45]. Accordingly, inter-odorant distances found
216 in the GCaMP bees were highly significantly correlated with those measured previously in OSNs using
217 calcium dye bath application (R^2 = 0.53, Mantel test p = 1.0e-4) or measured in PNs using dye injection
218 (R^2 = 0.44, Mantel test p = 1.0e-4). The correlation coefficients were not significantly different (R^2 =
219 0.53 vs. R^2 = 0.44, Fisher test, z = 0.98, p = 0.33, NS), suggesting the possibility that both OSN and PN
220 contribute to the signals recorded in the AL using genetically encoded GCaMP6f.

221 Finally, we asked if odorant response maps recorded with the GCaMP bees relate to bees'
222 actual perception of the odorants. We thus correlated the Euclidian distances measured between all
223 odor pairs in this study with distances measured in an appetitive conditioning experiment (S8 Data)
224 [48]. We found that behavioral distances can be predicted using signals recorded with genetically
225 encoded GCaMP6f (S6 Fig; R^2 = 0.34, Mantel test p = 1.0e-4). Thus, odorants evoking similar activity
226 patterns in the AL are treated as similar by honey bees in their behavior, a further confirmation that
227 GCaMP6f expression allows to record meaningful neural signals.

228

229 *Neural recordings in the lateral horn (LH)*

230 We then studied olfactory information processing in higher-order brain centers, first focusing
231 on the LH. All the aliphatic odorants used in this panel induced calcium signals in the LH (Fig 4A). Odor-
232 evoked signals systematically followed a biphasic time course, like that recorded in the AL (Fig 4B; S7
233 Fig; S6 Data). In the LH, all but one of the presented odorants induced a response that was significantly

234 higher than to the air control (S2 Data, n = 8 honey bees, RM-ANOVA, odor effect $F_{16,112}$ = 8.091, p =
235 0.0014, post hoc Dunnett tests, p < 0.04 except p = 0.09 for 2-hexanol). As in the AL, response
236 amplitudes correlated with odorants' vapor pressures (R^2 = 0.49, $F_{1,14}$ = 13.87, p = 0.0023). However,
237 this correlation appeared to be weaker in the LH with a near-significant difference between the two
238 correlation coefficients (R^2 = 0.84 in the AL vs. R^2 = 0.49 in the LH, Fisher test, z = 1.76, p = 0.078). In
239 other words, response intensity in the LH was not a simple product of the number of volatile molecules
240 in the odor puff, possibly revealing a yet undocumented gain control mechanism in the LH.

241 We then compared similarity relationships (Euclidian distances among odorants, S2 Data)
242 measured in the LH and in the AL and found a weak but still significant correlation (R^2 = 0.07, Mantel
243 test p = 0.023). This suggests a transformation of odor similarity relationships between the two
244 structures. A cluster analysis performed on Euclidian distances in the LH confirmed this finding. The
245 analysis roughly segregated alcohols (-OH moiety) on the one side and aldehydes/ketones (=O moiety)
246 on the other. However, different rules apply here, as the two longest chain molecules nonanal and 2-
247 nonanone clustered with the former group, while the shortest chain secondary alcohols, 2-hexanol
248 and 2 heptanol clustered with the latter group. Thus, the study of odor coding in the LH using GCaMP
249 bees suggests a less clear dependence on chemical features than in the AL.

250 Nevertheless, Euclidian distances measured in the LH correlated significantly with behavioral
251 distances measures [48] (R^2 = 0.12, Mantel test p = 0.0021), demonstrating that odorants evoking
252 similar activity patterns in the LH are treated as similar by honey bees in their behavior.

253

254 *Neural recordings in the mushroom bodies (MB)*

255 Lastly, we turned to the second higher-order center, the mushroom bodies (Fig 5, S3 Data), a
256 multisensory integration center in the honey bee brain. Calcium signals upon odorant presentation
257 were observed at the level of the calyx lip. Calcium signals systematically showed a biphasic time
258 course (Fig 5B; S8 Fig; S7 Data) like that recorded in the AL and in the LH, but in all cases with a small
259 first component and a much stronger second component. In this structure, the five presented odorants

260 induced significant activity in the MB calyx in comparison to the air control (Fig 5C; n = 6 honey bees,
261 RM-ANOVA, odor effect $F_{5,25}$ = 7.99, p = 0.0033, post hoc Dunnett tests p < 0.05, except 2-heptanone
262 with p = 0.07). However, the signal-to-noise ratio was considered too low for further analysis of inter-
263 odor relationships.
264
265 *Neural recordings of responses to social pheromones*
266 A condition for using GCaMP bees for unraveling the neural basis of social communication is
267 the ability to record robust responses to pheromonal odorants. We focused again on the LH and
268 presented a panel of honey bee pheromonal odorants, including both volatile (IPA, from the alarm
269 pheromone and ocimene, a volatile brood pheromone) and non-volatile compounds (queen and brood
270 pheromone compounds). Calcium signals were visible for all compounds in the LH (S4 Data, Fig 6A),
271 although the response intensity was significantly higher from the air control (Fig 6B, n = 7 honey bees)
272 for volatile compounds (t-tests, t > 4.35, p < 0.005) and for queen pheromone compounds (Friedman
273 ANOVA, odor effect F_{11} = 30.23, p = 0.0008; t-tests or Wilcoxon tests, t > 2.48, p < 0.05 except for 9-
274 ODA with t = 1.8 and p = 0.11) but not for brood pheromone compounds (t-tests t < 2.09, p = NS).
275
276 **DISCUSSION**
277 We developed a line of honey bees with pan-neuronal expression of a genetically-encoded
278 calcium sensor allowing to record neural activity from honey bee neurons. To our knowledge, this
279 represents the first neurogenetic tool for recording neural activity in a non-dipteran insect and eusocial
280 insect. Neurogenetic tools, especially the use of genetically-encoded calcium indicators (GECIs), have
281 been widely developed in both vertebrates [40, 49] and invertebrates [50] and supported major
282 progress in our understanding of the neural basis of behavior. In insects, such possibility was limited
283 until now to a few Dipteran species (fruit flies and mosquitoes [26]) and was lacking in other insects
284 with different lifestyles. The present development in a social Hymenoptera represents a major
285 progress for the neuroethology of social behavior but also a significant achievement in a species like

286 the honey bee in which neurogenetic tools are difficult to establish due to its peculiar reproductive
287 biology and the lack of knowledge of appropriate promoter sequences driving the expressions.

288 To develop our pan-neuronal calcium indicator, we expressed GCaMP6f under the control of
289 the promoter of the gene coding for synapsin, a vesicle–associated presynaptic protein found
290 throughout the honey bee brain [51]. This strategy was successful, as honey bees displayed broad
291 labeling with GCaMP6f in the major brain structures of the nervous system at sufficient amounts for
292 performing calcium imaging. Our neuroanatomical data confirm significant expression throughout the
293 bee brain (optic lobes, antennal lobe, mushroom bodies, and all other regions of the protocerebrum),
294 but we noticed substantial cell-to-cell variation in some regions, for instance in the cup of the
295 mushroom body calyx, which contains the somata of type I Kenyon cells (see Fig 1C): there, a strong
296 contrast appeared among neurons, suggesting differences in the level of GCaMP expression among
297 Kenyon cells or even some Kenyon cells lacking GCaMP expression. The GCaMP staining pattern did
298 not correspond to any of the Kenyon cell subtypes previously described based on their differing gene
299 expression profiles [52]. In contrast to the synapsin protein, GCaMP6f is located in the entire neuron,
300 since we detected staining in the somata (Fig 1C), the neurites, and the synaptic regions. This
301 widespread expression could represent a great advantage for performing functional recordings in the
302 bee brain.

303 To assess the power of this new tool for studying brain activity, we focused on the olfactory
304 system, which is the best-known sensory system in this animal. We compared the results obtained
305 using the GCaMP6f bees with previous results acquired using conventional dye injections or bath
306 application [19, 45]. For the first time, we could observe the simultaneous activation of the three main
307 brain structures involved in insect olfaction, the antennal lobe, the lateral horn, and the mushroom
308 body calyx.

309 While odor stimuli elicited responses well confined to these structures, also pure air stimuli
310 produced neuronal activation but distributed over further central brain regions. These could be
311 responses of various mechanosensory neurons, which in principle should be largely suppressed by the

312 olfactometer keeping a constant airflow. However, small fluctuations during the switching phases are
313 inevitable. Besides neuropils that process mechanosensory information from the Johnston's organ,
314 such as the dorsal lobe, the posterior protocerebral lobe, and the subesophageal zone [53], also MB
315 [54] and LH [55] are known to integrate mechanosensory information and recently mechanosensitivity
316 has also been reported in olfactory neurons [56, 57].

317 The possibility to record from different brain structures at the same time is a first and
318 important step towards the long-term goal to understand brain circuits responsible for bees'
319 sophisticated social behaviors and cognitive abilities, that may unravel yet undescribed sensory and/or
320 behavior-related pathways.

321 To follow this, we first validated our tool using individual structures and we confirmed its
322 validity for measuring relevant neural activity with regard to bees' behavior. Recordings obtained using
323 the GCaMP6f-expressing honey bees revealed the same olfactory coding rules in the AL as in previous
324 studies [19, 58]. Thus, odor-induced activity followed the same intensity rule (depending on the
325 odorant vapor pressure – Fig 3D), and inter-odorant neural distance measures were organized
326 according to odorants' chemical features, chain length, and functional group. Accordingly, calcium
327 imaging measured with the GCaMP-expressing bees allowed to predict how similarly honey bees
328 perceive these odorants, since inter-odor relationships among GCaMP response maps correlated with
329 inter-odor behavioral distances previously measured in an associative conditioning experiment [48].
330 This result, even if limited to a single sensory modality, is a strong confirmation of the biological
331 pertinence of the signals measured with this new neurogenetic tool.

332 In order to demonstrate that the activity can be followed to higher-order brain structures, we
333 studied the role of the lateral horn in encoding the chemical features of our odorants. The lateral horn
334 is a poorly studied structure in Hymenoptera, which could only be recorded previously using invasive
335 dye injection [59]. Importantly, while previous recordings only measured from a limited subpopulation
336 of projection neurons in this structure (the l-ALT), the GCaMP6f-expressing honey bees allowed
337 recording from the whole structure. The recordings in response to the 16 aliphatic odorants showed

338 that odor coding in this higher-order center is less clearly influenced by odorant quantity (*i.e.* lower
339 response amplitude differences among odorants) or by the chemical structure of the odorants than in
340 the AL. These first results suggest the existence of an additional gain control mechanism in this
341 structure, fitting with current discussions on its more diverse role in *Drosophila* [60]. This includes a
342 possible coding of hedonic odorant valence rather than chemical features [55, 61], a segregation of
343 food odors from pheromones [62], a central involvement in courtship behavior [63], or a multisensory
344 integration of olfactory, visual, mechanosensory, and gustatory information [55, 61]. The tool
345 presented here will allow for comparable studies also in the honey bee.

346 Calcium signals were also recorded in the mushroom body calyx, and odorants clearly activated
347 the lip, the olfactory input region of the calyx, as observed previously with a bath-applied dye [64]. The
348 signal amplitude was generally low, which reproduces the known sparseness of the MB odor code [65].
349 Together with the random arrangement of PN terminals and KC dendritic arbors in the lip, this
350 prevented the observation of odor-specific response maps at this point. However, advanced 3D
351 microscopy techniques [66] will benefit from this neurogenetic marker to unravel coding mechanisms
352 also in this neuropil, as experiments in *Drosophila* promise [67].

353 This new tool will provide a range of advantages over previous solutions. We expect that,
354 thanks to the genetically-encoded calcium sensor, it will facilitate imaging from other members of the
355 colony, like queens and drones, in contrast to what has been done until now (an exception is [68]).
356 Furthermore, it will also allow to extend the study of sensory processing to other sensory modalities
357 than the most commonly studied olfaction and vision. For instance, the study of mechanosensory
358 information processing notably used during the waggle dance remains limited [57, 69] and should be
359 facilitated using GCaMP-expressing honey bees. Lastly, transgenic bees could be instrumental for
360 studying neural signals in response to multisensory inputs, for instance in the mushroom bodies, the
361 higher-order center known for its role in multimodal sensory integration [70].

362 The future of insect neuroethology beyond the use of model organisms like *Drosophila* will
363 depend on the further development of neurogenetic tools in species like honey bees, with their rich

364 behavioral repertoire involving intricate social behaviors as well as elaborated cognitive skills. First, the
365 use of the CRISPR-Cas9 strategy, already developed in the honey bee [34], possibly allows target
366 specific insertion with an integration rate higher than the rate achieved with the PiggyBac transposon
367 system. It should be noted that once a transgenic queen is produced, the line can be kept for longer
368 periods of time by regularly raising new queens from the eggs laid by the initial queen. This procedure
369 involves relatively standard beekeeping practices. The future neurogenetic tools will also have to
370 improve the amplitudes of the calcium responses, with a better signal-to-noise ratio, a necessary
371 condition to study sensory coding in higher-order centers. A potential strategy would be to amplify the
372 GCaMP expression using the UAS-Gal4 or the Q binary expression systems commonly used in fruitflies
373 and mosquitoes [71]. Lastly, a better resolution will have to be achieved using cell-type-specific gene
374 expression to visualize (*i.e.* using fluorescent proteins such as GFP) or monitor activity (using GECIs as
375 here) from specific neuronal populations. The same precision shall then be exploited to silence or
376 activate specific neuron populations, allowing a temporal control of neural function. We hope that the
377 new line of GCaMP-expressing bees will represent the first step in this direction.
378
379
380 **MATERIAL AND METHODS**
381
382 ***PiggyBac* transgenesis**
383 The upstream promoter region together with the three exons of the 5' UTR of the honey bee *synapsin*
384 (*syn*) gene (LOC551737; assembly Amel_4.5, gene annotation 104) were successively cloned (S1 Fig).
385 This single fragment (1811 bp) was inserted into the PBac plasmid [33] using the *Asc*I/*Nco*I restriction
386 sites. The coding sequence of *GCaMP6f* was inserted downstream of the promoter region using
387 *Nco*I/*Mss*I restriction sites that finally resulted in the PBac [*syn-GCaMP6F*]Am plasmid. Requests for
388 the PBac [*syn-GCaMP6F*]Am plasmid should be directed to and will be fulfilled by Martin Beye
389 (martin.beye@hhu.de). Egg injections, larvae and queen rearing were performed following standard

390 methodology by employing the hyperactive transposase which we have customized for the honey bee
391 [33, 41]. A total of 4231 honey bee eggs not older than 1.5 h were injected, with 82% survival after
392 24h. Following the hatching, 34 eggs were reared to queens and only 7 out of the 34 were expressing
393 the GCaMP6f transgene. Semen from wild type drones was used for instrumental insemination of
394 queens. Inseminated queens were laying fertilized, usually female-determined eggs that were reared
395 either to queens or worker bees. Transgenic queens were identified by amplification of the transgene
396 in the offspring [41] using oligonucleotide primers (CCACACCTCCCCCTGAACCTGAAAC and
397 GAGGTAAGAATAAACATTGTTGGTC) targeting the PBac sequence. Only one inseminated queen was
398 kept for this study, and 2nd generation queens were reared from its offspring. Only 1% of the 2nd
399 generation queens were carrying the transgene suggesting that only a fraction of germ cells from the
400 1st queen carried the transgene. However, 50% of the offspring of the transgenic 2nd generation queens
401 were carrying the transgene, and workers were used for the anatomical staining and the calcium
402 imaging recordings.
403
404 **Anatomical immunostaining**
405 To visualize the expression pattern of the GCaMP6f in the honey bee brain, transgenic workers
406 were caught at emergence and were maintained in an incubator in the dark at 34°C for 2 weeks (*i.e.*
407 the same age as for calcium imaging). The brains of workers were dissected and immediately immersed
408 in cold 1% zinc formaldehyde in PBS (ZnFa 1% [72]) and kept overnight at 4°C. Brains were then washed
409 six times in PBS (10 min each), permeabilized in PBS containing 1% Triton X-100 for 30 min, and pre-
410 incubated 3h in PBS containing 0.3% Triton and 1% BSA (Bovine Serum Albumine in PBS, #37525,
411 ThermoScientific). To stain *GCaMP6f* and *synapsin* (as background staining), the brains were then
412 incubated in PBS containing 0.3% Triton and 0.1% BSA with rabbit polyclonal anti-GFP (Thermofisher,
413 #A-11122, France) at 1:100 dilution and mouse monoclonal anti-SYNORF1 (DHSB, #3C11, US) at 1:100
414 dilution for 7 days. Brains were then washed 6 times in PBS containing 0.3% Triton and incubated in
415 secondary antibodies directed against rabbit coupled to Alexa 488 (Thermofisher, #A11122, France)

416 and against mouse coupled to Alexa 555 (Thermofisher, #A-21147, France) both diluted at 1:200 for 5
417 days. Brains were then washed in PBS, dehydrated in an ascending ethanol series (30% to 100%),
418 cleared and finally mounted in methyl salicylate (M6752, Sigma-Aldrich, France) for observation. Brains
419 were scanned using a laser-scanning confocal microscope (Zeiss LSM 700) with a W Plan-Apochromat
420 20x/NA 1.0 objective using sequential excitation wavelengths of 488 nm and 555 nm, observing via
421 two color-filtered channels around 510 nm and 590 nm, respectively.
422
423 **Honey bee preparation for *in vivo* calcium imaging**
424 Transgenic workers were collected at emergence and were maintained in small cages in the
425 dark at 34°C for 2 weeks. On the day of the experiment, they were individually chilled on ice for 5 min
426 until they stopped moving. Then, they were prepared following the standard preparation used to
427 image the ventral part of the honey bee brain [19]. Briefly, the honey bee was fixed in a plastic chamber
428 with its antennae oriented to the front and the proboscis was fixed using beeswax to avoid movement
429 of the brain during the experiment. A pool was built with beeswax and pieces of plastic around the
430 head capsule, and a small window was then cut in the head cuticle. Glands as well as trachea were
431 removed to expose the brain, and the pool was filled with ringer solution (in mM: NaCl, 130; KCl, 6;
432 $MgCl_2$, 4; $CaCl_2$, 5; sucrose, 160; glucose, 25; Hepes, 10; pH 6.7, 500 mOsmol; all chemicals from Sigma-
433 Aldrich, France), to avoid desiccation of the brain surface. The honey bee was then left 30 min in a
434 moisturized and dark place before the calcium imaging.
435
436 **Calcium imaging**
437 A T.I.L.L. Photonics imaging system (Martinsried, Germany) was used to perform *in vivo* optical
438 recordings, as described elsewhere [19, 73, 74]. An epifluorescence microscope (Olympus BX51WI)
439 was used to record activity in the different regions of the brain with either a 4× dry objective (Olympus,
440 PlanCN; NA 0.10) for whole-brain recordings, a 10× water-immersion objective (Olympus, UMPlanFL;
441 NA 0.3) for AL and MB recordings or a 20x water-immersion objective (Olympus, UMPlanFL; NA 0.5)

442 for LH recordings. GCaMP6f was excited using 475 nm monochromatic light (T.I.L.L. Polychrom IV). The
443 fluorescence signal was separated by a 505 nm dichroic filter and a long-pass 515 nm emission filter
444 and recorded with a 640 × 480 pixels 12-bit monochrome CCD camera (T.I.L.L. Imago) cooled to -12°C
445 with 4 × 4 binning on chip. Each measurement consisted of 100 frames recorded at a rate of 5 Hz
446 (integration time for each frame ~50ms).
447
448 **Odor stimuli**
449 A constant airstream was directed from a distance of 1 cm to the bee's antennae, and odor
450 stimuli were given at the 15th frame for 1 s. For each odor stimulus (all obtained from Sigma-Aldrich,
451 France), 5 µL of the solution were deposited on a filter paper inserted in a Pasteur pipette. A pipette
452 containing a clean piece of filter paper was used as control stimulus.
453 For whole-brain recordings, we tested a small set of 3 odorant stimuli known from previous
454 work to trigger strong neural activity: 2-heptanone, octanal, and heptanal. For AL and LH recordings,
455 we tested 16 aliphatic odorants previously used in calcium imaging studies [19, 45] belonging to 4
456 functional groups (primary and secondary alcohols, aldehydes, and ketones) and having 4 different
457 carbon chain lengths (6, 7, 8, and 9 carbons). The use of these odorants which are part of floral blends
458 honey bees encounter while foraging [75] allowed to compare the results obtained in this study using
459 GCaMP6f imaging with previous studies using classical calcium-sensitive dyes such as Fura-2 dextran
460 [19] or Calcium green 2-AM [45]. These 16 odorants were used to record neural activity at the level of
461 the AL and at the level of the LH on two different groups of bees. For recordings at the level of the MB,
462 a reduced list of odorants which give strong neural activity was used: 1-hexanol, 2-hexanone, 2-
463 heptanone, heptanal, octanal, and the air control. For LH recordings in responses to social
464 pheromones, we tested both volatile (IPA and ocimene) and non-volatile compounds from the queen
465 pheromone (QMP, 9-ODA, 9-HDA, HOB and HVA) and from the brood pheromone (methyl oleate, ethyl
466 oleate, methyl linoleate, methyl palmitate, ethyl palmitate) at a concentration of 50µg/µL. As control
467 stimulus, a pipette containing the solvent (isopropanol) or a clean piece of filter paper was used.

468 Each odorant stimulus was presented twice in a pseudo-randomized order, avoiding the
469 consecutive presentation of stimuli with the same functional group or the same carbon chain length.
470 Only animals in which all odorants in the panel were presented were kept for analysis.
471
472 **Data processing and analyses**
473 All analyses were carried out using custom-made software written in IDL 6.0 (Research
474 Systems, Boulder, CO). Each odor response signal corresponds to a three-dimensional array consisting
475 of two spatial dimensions (*x*- and *y*-coordinates) along time (100 frames). First, the relative
476 fluorescence changes were calculated as $\Delta F/F = (F - F_0)/F_0$ by taking as reference background F_0 the
477 average of three frames just before the odorant stimulation (frames 9-11). Possible irregularities of
478 lamp illumination and bleaching were corrected by subtracting the median pixel value of each frame
479 from every single pixel of the corresponding frame. Finally, the two spatial dimensions were filtered
480 with a Gaussian filter of window size 7×7 pixels for AL recordings or 3×3 pixels for LH and MB recordings
481 for noise reduction. A biphasic calcium signal was observed in all recordings. As in previous studies
482 using bath-applied Calcium Green [45], a high contrast measure for the intensity of the odor-induced
483 response was obtained by averaging three consecutive frames at the end of the odor presentation
484 (frames 19-21) and subtracting the average of 3 frames during the second, negative component of the
485 signal (frames 49-51).
486 For the quantification of response intensity and similarity relationships, a mask was precisely
487 drawn in order to exclude regions outside of the imaged structure. A pixel-wise analysis was then
488 performed, using all the pixels within the mask. Response intensity was calculated by averaging the
489 intensity of all pixels located within the unmasked area. Similarity relationships between neural activity
490 patterns $I(x, y)$ were calculated by measuring Euclidian distances

491 $$d(o_1, o_2) = \sqrt{\sum_{x,y} (I_{o_1}(x, y) - I_{o_2}(x, y))^2}$$

492 for all the 120 odorant pairs o_1, o_2 within each animal.

493 For all analyses, average values for the two presentations of each odorant were used except
494 for the comparison of Euclidian distances for the same vs. different odorants (Fig 3E) in which each
495 single odorant presentation was used.
496 We used the Euclidian distances between odorants calculated using behavioral experiments
497 by Guerrieri *et al.* [48] to compare similarity relationships among odorants at the neural level with data
498 obtained at the behavioral level. All results are displayed as means over individuals ± SEM.
499
500 **Statistical analyses**
501 Odor response intensities were compared with ANOVA for repeated measurements, using
502 odors as within-group factors. A Dunnett post hoc test was applied to compare the intensity of the
503 response to each stimulus with a common reference, the air control. Responses to social pheromone
504 compounds were compared using a Friedman ANOVA. Wilcoxon matched-pairs tests were applied to
505 compare Euclidian distances between the same and different odors for AL recordings. Pearson
506 correlation analyses were performed between response intensity and the logarithm of odorants' vapor
507 pressure in mmHg (16 aliphatic odors recorded in the AL and in the LH) and between response
508 intensities recorded in this and previous studies (OSNs [45] or PNs [19]). A Fisher *z*-test was used to
509 test for significant differences between linear regression following Pearson correlation (R package
510 *multilevel*, *cordif* function). Mantel tests were used to compare matrices containing the Euclidian
511 distances for the 120 possible odor-pair among 16 odorants, either between different imaging studies,
512 or between neural and behavioral measures (R package *ade4*, *mantel.rtest* function). To explore
513 similarity relationships among odorants, hierarchical clustering using Ward's classification method was
514 used (R package *stats*, *hclust* function). All tests were performed with GraphPadPrism V7.00 and R
515 (www.r-project.org).
516
517
518 **ACKNOWLEDGEMENTS**

We thank Robin Parlow, Eva Theilenberg, Marion Müller-Borg, and Virginie Larcher for technical assistance. We thank Sara Bariselli for her support with the egg injection and Amélie Cabirol for fruitful discussions. We also thank Maud Combe for developing the custom programs used for data analysis. We thank the French Research National Agency (ANR to JCS, Project ANR-17-CE20-0003 Bee-O-Choc, Project ANR-22-CE37-0029 PHEROBRAIN), the CNRS (JCS) and the University Paris-Saclay (JC and JCS), the DFG (Deutsche Forschungsgemeinschaft to MB) and CIMeC, University of Trento (AH) for funding.

AUTHOR CONTRIBUTIONS

J.C., M.O., A.H., J.C.S., and M.B. conceived the experiments. J.C. and M.O. collected the data. J.C., M.O., A.H., J.C.S., and M.B. analyzed the data and interpreted the results. J.C., A.H., J.C.S., and M.B. wrote the manuscript. All authors read and approved the final version of the manuscript.

COMPETING INTEREST STATEMENT

The present research project was conducted in the absence of any commercial relationships that could be construed as a potential conflict of interest.

534 **FIGURE LEGENDS**

535

536 **Fig 1. Genetically encoded GCaMP6f and its neural expression**

537 **A-** Scheme of the honey bee *synapsin* promoter *GCaMP6f* expression cassette. CDS: coding sequence;
538 UTR: untranslated region; ATG: translation start. **B-** GCaMP6f expression in the honey bee brain
539 revealed by anti-GFP immunostaining (left, in green). GCaMP6f is widely expressed in the bee brain,
540 including in somata and neural tracts (white arrows). For comparison with *synapsin* expression, an anti-
541 SYNORF1 immunostaining (right, in red) is superimposed on the anti-GFP signal in green. Scale bar =
542 200 µm **C-** GCaMP6f expression (anti-GFP in green) and *synapsin* expression (anti-SYNORF1 in red) in
543 the antennal lobe. Remarkable and strong expression is observed in the somata of projection neurons
544 and local neurons (near the AL, white arrows). Scale bar = 50 µm. D- GCaMP6f expression (anti-GFP in
545 green) and *synapsin* expression (anti-SYNORF1 in red) in the mushroom bodies with strong expression
546 in some somata of Kenyon cells (in the cup of the calyces, see white arrows). Scale bar = 50 µm. AL:
547 Antennal lobe, MB: Mushroom body, OL: Optic lobe, Lo: Lobulla, Me: Medulla, vL: vertical lobe, lc:
548 lateral cluster of antennal lobe neuron somata, mc: medial cluster of antennal lobe neuron somata, Li:
549 Lip, BR: Basal ring, Co: Collar.

550

551 **Fig 2. Neural activity in the whole brain of the honey bee**

552 **A-** Hymenopteran olfactory pathway (adapted from [45]). Odorant molecules are detected by olfactory
553 sensory neurons (OSNs) on the antenna, which send olfactory information to the antennal lobe (AL).
554 Then, projection neurons (PNs) convey information to higher-order centers, the mushroom bodies
555 (MB) and the lateral horn (LH). Lo: Lobula, Me: Medulla, vL: vertical lobe, hL: horizontal lobe. **B-** Calcium
556 signals in the whole brain evoked by 3 different odorants (2-heptanone, octanal, heptanal) and the air
557 control. Relative fluorescence changes ($\Delta F/F$ [%]) are presented in a false-color code, from dark blue
558 (minimal response) to red (maximal response). **C-** Time course of odor-evoked responses ($\Delta F/F$ [%],
559 taken from the black squares shown in B) for one individual to the presentation of 2-heptanone (in

560 blue), octanal (in pink), and the air control (in grey), simultaneously recorded in the AL (left), the LH
561 (middle) and the MB (right). The calcium signals show a biphasic time course, with a fluorescence
562 increase upon odorant presentation (blue bars) followed by a long-lasting fluorescence undershoot, in
563 all brain regions.
564
565 **Fig 3. Neural activity recorded in the antennal lobe (AL)**
566 **A-** GCaMP6f calcium signals in the antennal lobe evoked by a panel of 16 odorants varying
567 systematically according to their carbon chain length (C6–C9) and their functional group (primary and
568 secondary alcohols, aldehydes, and ketones). Different odorants induce different glomerular activity
569 patterns. The map shows the whole amplitude of the response including both positive and negative
570 components (see text for calculation). **B-** Example time courses (top, taken from the black square
571 shown in A in C7 ketones) and average time courses (bottom, n = 11 honey bees) of odor-evoked
572 responses ($\Delta F/F$ [%]) recorded in the AL to 2-heptanone (in red), octanal (in blue), and to the air control
573 (in grey). **C-** Amplitude of calcium responses ($\Delta F/F$ [%]) to the 16 aliphatic odorants and to the air
574 control. All odorants induce significant activity in comparison to the air control (n = 11 honey bees, **
575 $p < 0.0097$). The intensity of the odor-induced response was obtained by averaging three consecutive
576 frames at the end of the odor presentation (frames 19-21) and subtracting the average of 3 frames
577 during the second, negative component of the signal (frames 49-51). **D-** Amplitude of calcium
578 responses ($\Delta F/F$ [%]) as a function of odorant vapor pressure (in log units). The linear regression shows
579 a significant correlation (R^2 = 0.84, *** p = 6e-7). **E-** Different presentations of the same odorants (2-
580 octanone and heptanal) show similar glomerular patterns in the AL (left). Dissimilarity measures
581 (Euclidian distance, right) between representations of the same or of different odorants. Activity maps
582 are more similar (shorter distances) when the same odorant is presented (*** p = 1.1e-4), showing, as
583 expected, a clear odor coding in this structure. **F-** Cluster analysis showing similarity relationships
584 among odorants (Ward's classification method). Functional groups are shown in different colors:
585 primary alcohols in blue, secondary alcohols in green, aldehydes in black, and ketones in red. The

586 analysis shows a first separation between odorants with short and long carbon chain lengths. Odorants
587 with a short carbon chain are then subdivided into alcohols (primary and secondary, C-OH functional
588 group) and ketones/aldehydes (C=O functional group). The data underlying the graphs shown in the
589 figure can be found in S1 Data and S5 Data.
590
591 **Fig 4. Neural activity recorded in the lateral horn (LH)**
592 **A-** Calcium signals in the lateral horn evoked by the same panel of 16 odorants. Different odorants
593 induce different activity patterns in the LH. **B-** Example time courses (top, taken from the black square
594 shown in A in C7 ketones) and average time courses (bottom, n = 8 honey bees) of odor-evoked
595 responses ($\Delta F/F$ [%]) recorded in the LH (in the black square shown in A) to 2-heptanone (in red),
596 octanal (in blue), and to the air control (in grey). The calcium signals also show a biphasic response,
597 with a fluorescence increase upon odor presentation (blue bar) followed by a long undershoot. **C-**
598 Amplitude of calcium responses ($\Delta F/F$ [%]) to the 16 aliphatic odorants and to the air control. All
599 odorants induce a significant activity in comparison to the air control (n = 8 honey bees, * $p < 0.04$). **D-**
600 Cluster analysis showing similarity relationships among odorants (Ward's classification method). The
601 data underlying the graphs shown in the figure can be found in S2 Data and S6 Data.
602
603 **Fig 5. Neural activity recorded in the mushroom bodies (MB)**
604 **A**- Calcium signals in the calyces of the mushroom bodies in response to the presentations of 2-
605 heptanone, heptanal, octanal, and the air control. **B-** Example time courses (left, taken from the black
606 square shown in A in 2-heptanone) or average time courses (right, n = 6 honey bees) of odor-evoked
607 responses ($\Delta F/F$ [%]) recorded in the lip of the MB (black square shown in A) to 2-heptanone (in red),
608 octanal (in blue), and to the air control (in grey). Calcium signals are weaker here than in other
609 structures, with a smaller first component and a larger second component. **C-** Amplitude of calcium
610 responses ($\Delta F/F$ [%]) to the 5 tested odorants and to the air control. All odorants induce significant

activity in comparison to the air control (n = 6 honey bees, * $p < 0.05$, except 2-heptanone with p =0.07). The data underlying the graphs shown in the figure can be found in S3 Data and S7 Data.

Fig 6. Neural responses to pheromonal odorants recorded in the lateral horn

A- GCaMP6f calcium signals in the lateral horn evoked by a panel of pheromonal compounds, both volatile (IPA and ocimene in black) or not volatile (queen pheromone compounds in red and brood pheromone compounds in blue) and to the controls (isopropanol and air). Different odorants induce activity patterns. Relative fluorescence changes ($\Delta F/F$ [%]) are presented in a false-color code (see colorbar), from dark blue (minimal response) to red (maximal response). **B-** Amplitude of calcium responses ($\Delta F/F$ [%]) to the 12 tested odorants and to the controls (air and isopropanol). Volatile odorants and queen pheromone compounds induce significant activity in comparison to the controls (n = 7 honey bees, * $p < 0.05$). The data underlying the graphs shown in the figure can be found in S4 Data.

637 **REFERENCES**

638 1. Bourke AFG. Principles of Social Evolution. Oxford University Press; 2011.
639 2. Hamilton WD. The genetical evolution of social behaviour. II. J Theor Biol. 1964;7: 17–52.
640 doi:10.1016/0022-5193(64)90039-6
641 3. Hölldobler B, Wilson EO. The Ants. Cambridge: Harvard University Press; 1990.
642 4. Wilson EO. The social conquest of earth. WW Norton & Company; 2012.
643 5. Oster GF, Wilson EO. Caste and ecology in the social insects. Princeton, New Jersey: Princeton
644 University Press.; 1978.
645 6. Paoli M, Galizia GC. Olfactory coding in honeybees. Cell Tissue Res. 2021;383: 35–58.
646 doi:10.1007/s00441-020-03385-5
647 7. Woodgate JL, Makinson JC, Rossi N, Lim KS, Reynolds AM, Rawlings CJ, et al. Harmonic radar
648 tracking reveals that honeybee drones navigate between multiple aerial leks. iScience. 2021;24:
649 102499. doi:10.1016/j.isci.2021.102499
650 8. Avarguès-Weber A, Dyer AG, Combe M, Giurfa M. Simultaneous mastering of two abstract
651 concepts by the miniature brain of bees. Proc Natl Acad Sci. 2012;109: 7481–7486.
652 doi:10.1073/pnas.1202576109
653 9. Cholé H, Carcaud J, Mazeau H, Famié S, Arnold G, Sandoz J-C. Social Contact Acts as Appetitive
654 Reinforcement and Supports Associative Learning in Honeybees. Curr Biol. 2019;29: 1407-
655 1413.e3. doi:10.1016/j.cub.2019.03.025
656 10. Barron AB, Plath JA. The evolution of honey bee dance communication: a mechanistic
657 perspective. J Exp Biol. 2017;220: 4339–4346. doi:10.1242/jeb.142778
658 11. Giurfa M, Sandoz JC. Invertebrate learning and memory: Fifty years of olfactory conditioning of
659 the proboscis extension response in honeybees. Learn Mem. 2012;19: 54–66.
660 doi:10.1101/lm.024711.111
661 12. Wycke M-A, Coureaud G, Thomas-Danguin T, Sandoz J-C. Configural perception of a binary
662 olfactory mixture in honey bees as in humans, rodents and newborn rabbits. J Exp Biol. 2020;223:
663 jeb227611. doi:10.1242/jeb.227611
664 13. Paoli M, Albi A, Zanon M, Zanini D, Antolini R, Haase A. Neuronal Response Latencies Encode First
665 Odor Identity Information across Subjects. J Neurosci. 2018;38: 9240–9251.
666 doi:10.1523/JNEUROSCI.0453-18.2018
667 14. Farris SM. Insect societies and the social brain. Curr Opin Insect Sci. 2016;15: 1–8.
668 doi:10.1016/j.cois.2016.01.010
669 15. Lihoreau M, Latty T, Chittka L. An Exploration of the Social Brain Hypothesis in Insects. Front
670 Physiol. 2012;3. doi:10.3389/fphys.2012.00442
671 16. Cabirol A, Brooks R, Groh C, Barron AB, Devaud J. Experience during early adulthood shapes the
672 learning capacities and the number of synaptic boutons in the mushroom bodies of honey bees
673 (Apis mellifera). Learn Mem. 2017;24: 557–562. doi:10.1101/lm.045492.117
674 17. Suenami S, Iino S, Kubo T. Pharmacologic inhibition of phospholipase C in the brain attenuates
675 early memory formation in the honeybee (Apis mellifera L.). Biol Open. 2018;7: bio028191.
676 doi:10.1242/bio.028191
677 18. Duer A, Paffhausen BH, Menzel R. High order neural correlates of social behavior in the
678 honeybee brain. J Neurosci Methods. 2015;254: 1–9. doi:10.1016/j.jneumeth.2015.07.004
679 19. Carcaud J, Giurfa M, Sandoz JC. Differential Processing by Two Olfactory Subsystems in the
680 Honeybee Brain. Neuroscience. 2018;374: 33–48. doi:10.1016/j.neuroscience.2018.01.029
681 20. Haase A, Rigosi E, Frasnelli E, Trona F, Tessarolo F, Vinegoni C, et al. A multimodal approach for
682 tracing lateralisation along the olfactory pathway in the honeybee through electrophysiological

683 recordings, morpho-functional imaging, and behavioural studies. Eur Biophys J. 2011;40: 1247–
684 1258. doi:10.1007/s00249-011-0748-6
685 21. Sherer LM, Certel SJ. The fight to understand fighting: neurogenetic approaches to the study of
686 aggression in insects. Curr Opin Insect Sci. 2019;36: 18–24. doi:10.1016/j.cois.2019.06.004
687 22. McKelvey EG, Fabre CC. Recent neurogenetic findings in insect courtship behaviour. Curr Opin
688 Insect Sci. 2019;36: 103–110. doi:10.1016/j.cois.2019.08.010
689 23. Ehmann N, Pauls D. Optogenetics: Illuminating neuronal circuits of memory formation. J
690 Neurogenet. 2020;34: 47–54. doi:10.1080/01677063.2019.1708352
691 24. Sadanandappa MK, Sathyanarayana SH, Kondo S, Bosco G. Neuropeptide F signaling regulates
692 parasitoid-specific germline development and egg-laying in Drosophila. PLOS Genet. 2021;17:
693 e1009456. doi:10.1371/journal.pgen.1009456
694 25. Pooryasin A, Maglione M, Schubert M, Matkovic-Rachid T, Hasheminasab S, Pech U, et al.
695 Unc13A and Unc13B contribute to the decoding of distinct sensory information in Drosophila.
696 Nat Commun. 2021;12: 1932. doi:10.1038/s41467-021-22180-6
697 26. Grover D, Katsuki T, Li J, Dawkins TJ, Greenspan RJ. Imaging brain activity during complex social
698 behaviors in Drosophila with Flyception2. Nat Commun. 2020;11: 623. doi:10.1038/s41467-020-
699 14487-7
700 27. Jové V, Gong Z, Hol FJH, Zhao Z, Sorrells TR, Carroll TS, et al. Sensory Discrimination of Blood and
701 Floral Nectar by Aedes aegypti Mosquitoes. Neuron. 2020;108: 1163-1180.e12.
702 doi:10.1016/j.neuron.2020.09.019
703 28. Vinauger C, Van Breugel F, Locke LT, Tobin KKS, Dickinson MH, Fairhall AL, et al. Visual-Olfactory
704 Integration in the Human Disease Vector Mosquito Aedes aegypti. Curr Biol. 2019;29: 2509-
705 2516.e5. doi:10.1016/j.cub.2019.06.043
706 29. Koutroumpa FA, Monsempes C, François M-C, de Cian A, Royer C, Concordet J-P, et al. Heritable
707 genome editing with CRISPR/Cas9 induces anosmia in a crop pest moth. Sci Rep. 2016;6: 29620.
708 doi:10.1038/srep29620
709 30. Fandino RA, Alexander Haverkamp, Bisch-Knaden S, Zhang J, Bucks S, Tu Anh Thi Nguyen, et al.
710 Mutagenesis of odorant coreceptor Orco fully disrupts foraging but not oviposition behaviors in
711 the hawkmoth Manduca sexta. Proc Natl Acad Sci U S A. 2019;116.
712 doi:10.1073/pnas.1902089116
713 31. DeGennaro M, McBride CS, Seeholzer L, Nakagawa T, Dennis EJ, Goldman C, et al. orco mutant
714 mosquitoes lose strong preference for humans and are not repelled by volatile DEET. Nature.
715 2013;498: 487–491. doi:10.1038/nature12206
716 32. McMeniman CJ, Corfas RA, Matthews BJ, Ritchie SA, Vosshall LB. Multimodal Integration of
717 Carbon Dioxide and Other Sensory Cues Drives Mosquito Attraction to Humans. Cell. 2014;156:
718 1060–1071. doi:10.1016/j.cell.2013.12.044
719 33. Zhang Z-J, Zhang S-S, Niu B-L, Ji D-F, Liu X-J, Li M-W, et al. A determining factor for insect feeding
720 preference in the silkworm, Bombyx mori. PLOS Biol. 2019;17: e3000162.
721 doi:10.1371/journal.pbio.3000162
722 34. Schulte C, Theilenberg E, Muller-Borg M, Gempe T, Beye M. Highly efficient integration and
723 expression of piggyBac-derived cassettes in the honeybee (Apis mellifera). Proc Natl Acad Sci.
724 2014;111: 9003–9008. doi:10.1073/pnas.1402341111
725 35. Roth A, Vleurinck C, Netschitailo O, Bauer V, Otte M, Kaftanoglu O, et al. A genetic switch for
726 worker nutrition-mediated traits in honeybees. PLOS Biol. 2019;17: e3000171.
727 doi:10.1371/journal.pbio.3000171
728 36. Chen Z, Traniello IM, Rana S, Cash-Ahmed AC, Sankey AL, Yang C, et al. Neurodevelopmental and
729 transcriptomic effects of CRISPR/Cas9-induced somatic orco mutation in honey bees. J
730 Neurogenet. 2021;35: 320–332. doi:10.1080/01677063.2021.1887173

37. Değirmenci L, Geiger D, Rogé Ferreira FL, Keller A, Krischke B, Beye M, et al. CRISPR/Cas 9-Mediated Mutations as a New Tool for Studying Taste in Honeybees. Chem Senses. 2020;45: 655–666. doi:10.1093/chemse/bjaa063
38. Nie H-Y, Liang L-Q, Li Q-F, Li Z-H-Q, Zhu Y-N, Guo Y-K, et al. CRISPR/Cas9 mediated knockout of Amyellow-y gene results in melanization defect of the cuticle in adult Apis mellifera. J Insect Physiol. 2021;132: 104264. doi:10.1016/j.jinsphys.2021.104264
39. Wang JW, Wong AM, Flores J, Vosshall LB, Axel R. Two-photon calcium imaging reveals an odor-evoked map of activity in the fly brain. Cell. 2003;112: 271–282. doi:10.1016/S0092-8674(03)00004-7
40. Muto A, Ohkura M, Kotani T, Higashijima S, Nakai J, Kawakami K. Genetic visualization with an improved GCaMP calcium indicator reveals spatiotemporal activation of the spinal motor neurons in zebrafish. Proc Natl Acad Sci. 2011;108: 5425–5430. doi:10.1073/pnas.1000887108
41. Chen T-W, Wardill TJ, Sun Y, Pulver SR, Renninger SL, Baohan A, et al. Ultrasensitive fluorescent proteins for imaging neuronal activity. Nature. 2013;499: 295–300. doi:10.1038/nature12354
42. Otte M, Netschitailo O, Kaftanoglu O, Wang Y, Page RE, Beye M. Improving genetic transformation rates in honeybees. Sci Rep. 2018;8: 1–6. doi:10.1038/s41598-018-34724-w
43. Strausfeld NJ. Organization of the honey bee mushroom body: Representation of the calyx within the vertical and gamma lobes. J Comp Neurol. 2002;450: 4–33. doi:10.1002/cne.10285
44. Suenami S, Oya S, Kohno H, Kubo T. Kenyon Cell Subtypes/Populations in the Honeybee Mushroom Bodies: Possible Function Based on Their Gene Expression Profiles, Differentiation, Possible Evolution, and Application of Genome Editing. Front Psychol. 2018;9. doi:10.3389/fpsyg.2018.01717
45. Joerges J, Küttner A, Galizia CG, Menzel R. Representations of odours and odour mixtures visualized in the honeybee brain. Nature. 1997;387: 285–288. doi:10.1038/387285a0
46. Carcaud J, Hill T, Giurfa M, Sandoz J-C. Differential coding by two olfactory subsystems in the honey bee brain. J Neurophysiol. 2012; 1106–1121. doi:10.1152/jn.01034.2011
47. Galizia CG, Nägler K, Hölldobler B, Menzel R. Odour coding is bilaterally symmetrical in the antennal lobes of honeybees (Apis mellifera). Eur J Neurosci. 1998;10: 2964–2974. doi:10.1111/j.1460-9568.1998.00303.x
48. Sachse S, Galizia CG. Role of inhibition for temporal and spatial odor representation in olfactory output neurons: a calcium imaging study. J Neurophysiol. 2002;87: 1106–1117. doi:11826074
49. Guerrieri F, Schubert M, Sandoz J-C, Giurfa M. Perceptual and Neural Olfactory Similarity in Honeybees. PLoS Biol. 2005;3: e60. doi:10.1371/journal.pbio.0030060
50. Lin MZ, Schnitzer MJ. Genetically encoded indicators of neuronal activity. Nat Neurosci. 2016;19: 1142–1153. doi:10.1038/nn.4359
51. Dana H, Sun Y, Mohar B, Hulse BK, Kerlin AM, Hasseman JP, et al. High-performance calcium sensors for imaging activity in neuronal populations and microcompartments. Nat Methods. 2019;16: 649–657. doi:10.1038/s41592-019-0435-6
52. Groh C, Lu Z, Meinertzhagen IA, Rössler W. Age-related plasticity in the synaptic ultrastructure of neurons in the mushroom body calyx of the adult honeybee Apis mellifera. J Comp Neurol. 2012;520: 3509–3527. doi:10.1002/cne.23102
53. Ai H. Vibration-processing interneurons in the honeybee brain. Front Syst Neurosci. 2010;3: 1–10. doi:10.3389/neuro.06.019.2009
54. Mobbs PG. The brain of the honeybee Apis mellifera. I. The connections and spatial organization of the mushroom bodies. Philos Trans R Soc London B, Biol Sci. 1982;298: 309–354. doi:10.1098/rstb.1982.0086

55. Dolan MJ, Frechter S, Bates AS, Dan C, Huoviala P, Roberts RJ, et al. Neurogenetic dissection of the drosophila lateral horn reveals major outputs, diverse behavioural functions, and interactions with the mushroom body. Elife. 2019;8: 1–45. doi:10.7554/eLife.43079
56. Tuckman H, Kim J, Rangan A, Lei H, Patel M. Dynamics of sensory integration of olfactory and mechanical stimuli within the response patterns of moth antennal lobe neurons. J Theor Biol. 2021;509: 110510. doi:10.1016/j.jtbi.2020.110510
57. Tiraboschi E, Leonardelli L, Segata G, Haase A. Parallel Processing of Olfactory and Mechanosensory Information in the Honey Bee Antennal Lobe. Front Physiol. 2021;12: 2021.05.11.443598. doi:10.3389/fphys.2021.790453
58. Sachse S, Rappert A, Galizia CG. The spatial representation of chemical structures in the antennal lobe of honeybees: Steps towards the olfactory code. Eur J Neurosci. 1999;11: 3970–3982. doi:10.1046/j.1460-9568.1999.00826.x
59. Roussel E, Carcaud J, Combe M, Giurfa M, Sandoz J-C. Olfactory Coding in the Honeybee Lateral Horn. Curr Biol. 2014;24: 561–567. doi:10.1016/j.cub.2014.01.063
60. Schultzhaus JN, Saleem S, Iftikhar H, Carney GE. The role of the Drosophila lateral horn in olfactory information processing and behavioral response. J Insect Physiol. 2017;98: 29–37. doi:10.1016/j.jinsphys.2016.11.007
61. Strutz A, Soelter J, Baschwitz A, Farhan A, Grabe V, Rybak J, et al. Decoding odor quality and intensity in the Drosophila brain. Elife. 2014;3: e04147. doi:10.7554/eLife.04147
62. Jefferis GSXE, Potter CJ, Chan AM, Marin EC, Rohlfing T, Maurer CR, et al. Comprehensive Maps of Drosophila Higher Olfactory Centers: Spatially Segregated Fruit and Pheromone Representation. Cell. 2007;128: 1187–1203. doi:10.1016/j.cell.2007.01.040
63. Kido A, Ito K. Mushroom bodies are not required for courtship behavior by normal and sexually mosaic Drosophila. J Neurobiol. 2002;52: 302–311. doi:10.1002/neu.10100
64. Faber T, Menzel R. Visualizing mushroom body response to a conditioned odor in honeybees. Naturwissenschaften. 2001;88: 472–476. doi:10.1007/s001140100263
65. Szyszka P, Ditzen M, Galkin A, Galizia CG, Menzel R. Sparsening and temporal sharpening of olfactory representations in the honeybee mushroom bodies. J Neurophysiol. 2005;94: 3303–13. doi:10.1152/jn.00397.2005
66. Paoli M, Haase A. In Vivo Two-Photon Imaging of the Olfactory System in Insects. In: Simoes de Souza F. AG, editor. Olfactory Receptors. New York: Humana Press; 2018. pp. 179–219. doi:10.1007/978-1-4939-8609-5_15
67. Bilz F, Geurten BRH, Hancock CE, Widmann A, Fiala A. Visualization of a Distributed Synaptic Memory Code in the Drosophila Brain. Neuron. 2020;106: 963-976.e4. doi:10.1016/j.neuron.2020.03.010
68. Sandoz J-C. Odour-evoked responses to queen pheromone components and to plant odours using optical imaging in the antennal lobe of the honey bee drone Apis mellifera L. J Exp Biol. 2006;209: 3587–3598. doi:10.1242/jeb.02423
69. Ai H, Kai K, Kumaraswamy A, Ikeno H, Wachtler T. Interneurons in the Honeybee Primary Auditory Center Responding to Waggle Dance-Like Vibration Pulses. J Neurosci. 2017;37: 10624–10635. doi:10.1523/JNEUROSCI.0044-17.2017
70. Groh C, Rössler W. Analysis of Synaptic Microcircuits in the Mushroom Bodies of the Honeybee. Insects. 2020;11: 43. doi:10.3390/insects11010043
71. Zhao Z, Tian D, McBride CS. Development of a pan-neuronal genetic driver in Aedes aegypti mosquitoes. Cell Reports Methods. 2021;1: 100042. doi:10.1016/j.crmeth.2021.100042
72. Ott SR. Confocal microscopy in large insect brains: Zinc–formaldehyde fixation improves synapsin immunostaining and preservation of morphology in whole-mounts. J Neurosci Methods. 2008;172: 220–230. doi:10.1016/j.jneumeth.2008.04.031

73. Carcaud J, Giurfa M, Sandoz J-C. Differential Combinatorial Coding of Pheromones in Two Olfactory Subsystems of the Honey Bee Brain. J Neurosci. 2015;35: 4157–4167. doi:10.1523/JNEUROSCI.0734-14.2015
74. Haehnel M, Froese A, Menzel R. In vivo Ca2+- Imaging of mushroom body neurons during olfactory learning in the honey bee. J Vis Exp. 2009; e1353. doi:10.3791/1353
75. Knudsen JT, Tollsten L, Bergström LG. Floral scents—a checklist of volatile compounds isolated by head-space techniques. Phytochemistry. 1993;33: 253–280. doi:10.1016/0031-9422(93)85502-I

860 **SUPPORTING INFORMATION**

861 **S1 Fig. Synapsin promoter sequence of the honey bee**

862 The upstream promoter region and the 5' UTR sequence of the honey bee *synapsin* (*syn*) gene as
863 revealed from the gene annotation release 104 (NCBI Apis mellifera Annotation Release 104;
864 https://www.ncbi.nlm.nih.gov/genome/annotation_euk/Apis_mellifera/104/). In grey the predicted
865 promoter and upstream region. Different colors indicate the different annotated exons that were
866 fused to obtain a single 5'UTR region.

867

868 **S2 Fig. Comparison of immunostaining of GCaMP6f in different honey bees**

869 **A-** GCaMP6f expression (anti-GFP in green) in the AL of different honey bees showing strong expression
870 in the somata of projection neurons and local neurons (white arrows). **B**- GCaMP6f expression (anti-
871 GFP in green) in the mushroom bodies in different honey bees showing strong expression in somata of
872 the Kenyon cells (in the cup of the calyces, see white arrows). Scale bar = 50 µm. AL: Antennal lobe,
873 MB: Mushroom body, Li: Lip, BR: Basal ring, Co: Collar. **C**- Examples of AL and MB of wild type (WT)
874 bees showing no GCaMP6f expression.

875

876 **S3 Fig. GCaMP6f expression in different regions**

877 **A-** GCaMP6f expression (anti-GFP in green) in the lateral cluster of local/projection neurons near the
878 AL (left) and its zoom (right), showing very broad expression in almost all the somata. Scale bar = 50
879 µm. AL: Antennal lobe. **B**- GCaMP6f expression (anti-GFP in green) in the photoreceptors of the ocelli.
880 MB: Mushroom body.

881

882 **S4 Fig. Time-courses of odor-evoked responses recorded in the antennal lobe**

883 A- Time course of odor-evoked responses ($\Delta F/F$ [%]) recorded in the AL (n = 11 honey bees) to different
884 odorants and the air control (in grey). Time course with no olfactory stimulation (n = 2 honey bees) is
885 also shown (in grey). B- Time course ($\Delta F/F$ [%]) recorded in the AL of wild type bees (n = 10 honey bees)

886 following odor presentations, showing no signal in non-transgenic bees. The data underlying the
887 graphs shown in the figure can be found in S5 Data.
888
889 **S5 Fig. Correlation between amplitudes of calcium responses recorded in the antennal lobe**
890 **A-** Amplitude of calcium responses ($\Delta F/F$ [%]) recorded in Olfactory sensory neurons (OSNs) in [45] as
891 a function of the amplitude of calcium responses ($\Delta F/F$ [%]) recorded in the AL in this study. The linear
892 regression shows a significant correlation ($R^2 = 0.84$, *** $p = 6e\text{-}7$). **B-** Amplitude of calcium responses
893 ($\Delta F/F$ [%]) recorded in Projection neurons (PNs) in [19] as a function of the amplitude of calcium
894 responses ($\Delta F/F$ [%]) recorded in the AL in this study. The linear regression shows a significant
895 correlation ($R^2 = 0.78$, *** $p = 6e\text{-}6$).
896
897 **S6 Fig. Correlation between neural and behavioral distances**
898 Correlation of Euclidian distances recorded in the AL in this study are highly correlated with behavioral
899 distances recorded in (48) ($R^2 = 0.34$, *** $p < 0.001$). The data underlying the graphs shown in the figure
900 can be found in S8 Data.
901
902 **S7 Fig. Time-courses of odor-evoked responses recorded in the lateral horn**
903 Time course of odor-evoked responses ($\Delta F/F$ [%]) recorded in the LH ($n = 8$ honey bees) to the different
904 odorants and to the air control (in grey). The data underlying the graphs shown in the figure can be
905 found in S6 Data.
906
907 **S8 Fig. Time-courses of odor-evoked responses recorded in the mushroom bodies**
908 Time course of odor-evoked responses ($\Delta F/F$ [%]) recorded in the MB ($n = 6$ honey bees) to the
909 different odorants and to the air control (in grey). The data underlying the graphs shown in the figure
910 can be found in S7 Data.
911

S1 Data. Calcium imaging data recorded in the antennal lobe. Data underlying Fig 3.

S2 Data. Calcium imaging data recorded in the lateral horn. Data underlying Fig 4.

S3 Data. Calcium imaging data recorded in the mushroom bodies. Data underlying Fig 5.

S4 Data. Calcium imaging data recorded in the lateral horn in response to pheromonal compounds. Data underlying Fig 6.

S5 Data. Timecourses data recorded in the antennal lobe. Data underlying Fig 3B.

S6 Data. Timecourses data recorded in the lateral horn. Data underlying Fig 4B.

S7 Data. Timecourses data recorded in the mushroom bodies. Data underlying Fig 5B.

S8 Data. Behavioral Euclidian distances. From Guerrieri et al. 2005; Data underlying S6 Fig.

Figure 1

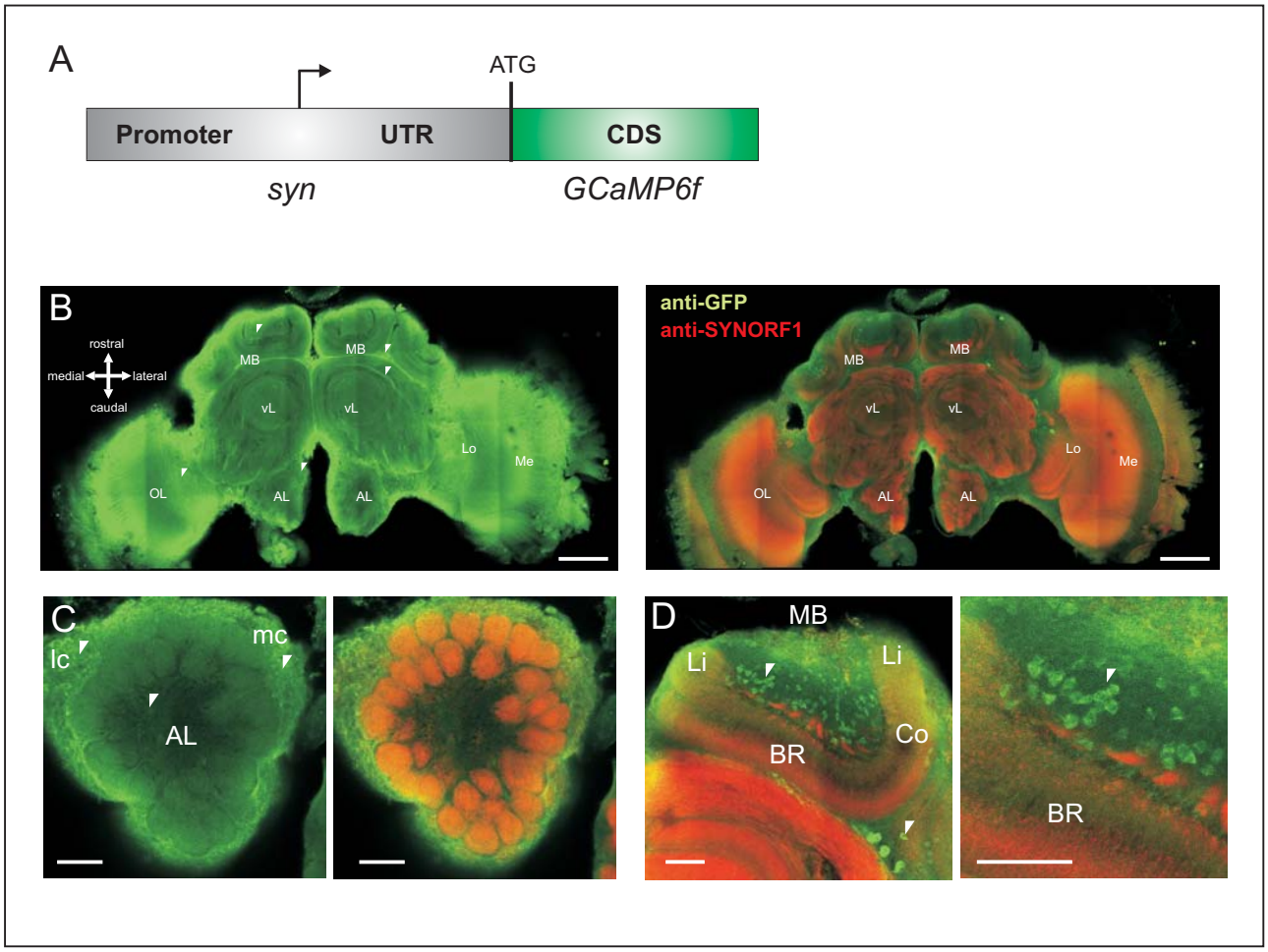
A
ATG
Promoter
UTR
CDS
syn
GCaMP6f
B
rostral
medial
lateral
caudal
MB
MB
vL
vL
Lo
Me
OL
AL
AL
anti-GFP
anti-SYNORF1
MB
MB
vL
vL
Lo
Me
OL
AL
AL
C
lc
mc
AL
D
MB
Li
Li
Co
BR
BR

Figure 2

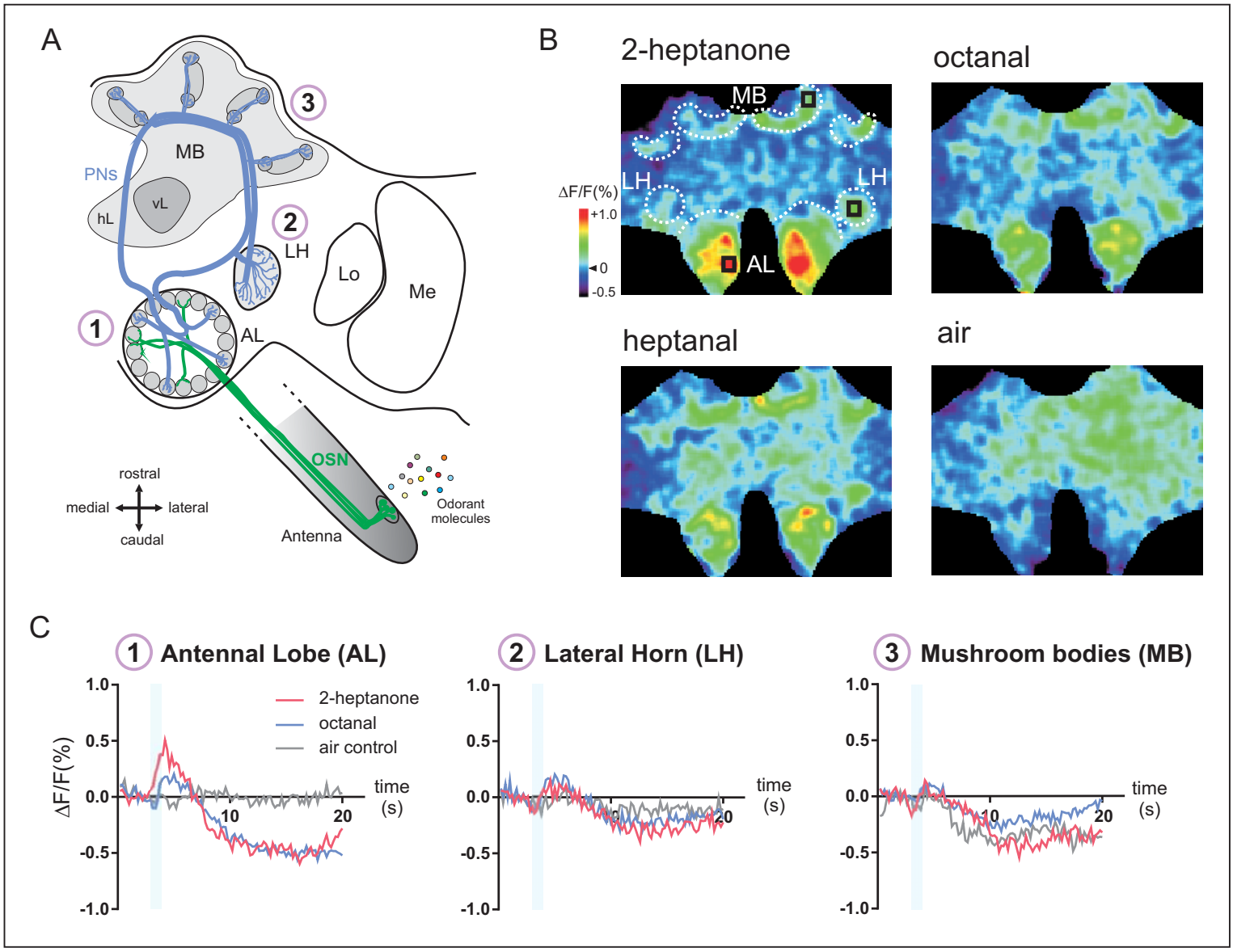
A
MB
PNs
vL
hL
3
2
LH
Lo
Me
1
AL
OSN
rostral
medial
lateral
caudal
Antenna
Odorant molecules
B
2-heptanone
octanal
heptanal
air
MB
LH
LH
AL
ΔF/F(%)
+1.0
0
-0.5
C
1 Antennal Lobe (AL)
2 Lateral Horn (LH)
3 Mushroom bodies (MB)
2-heptanone
octanal
air control
ΔF/F(%)
1.0
0.5
0.0
-0.5
-1.0
10
20
time (s)

Figure 3

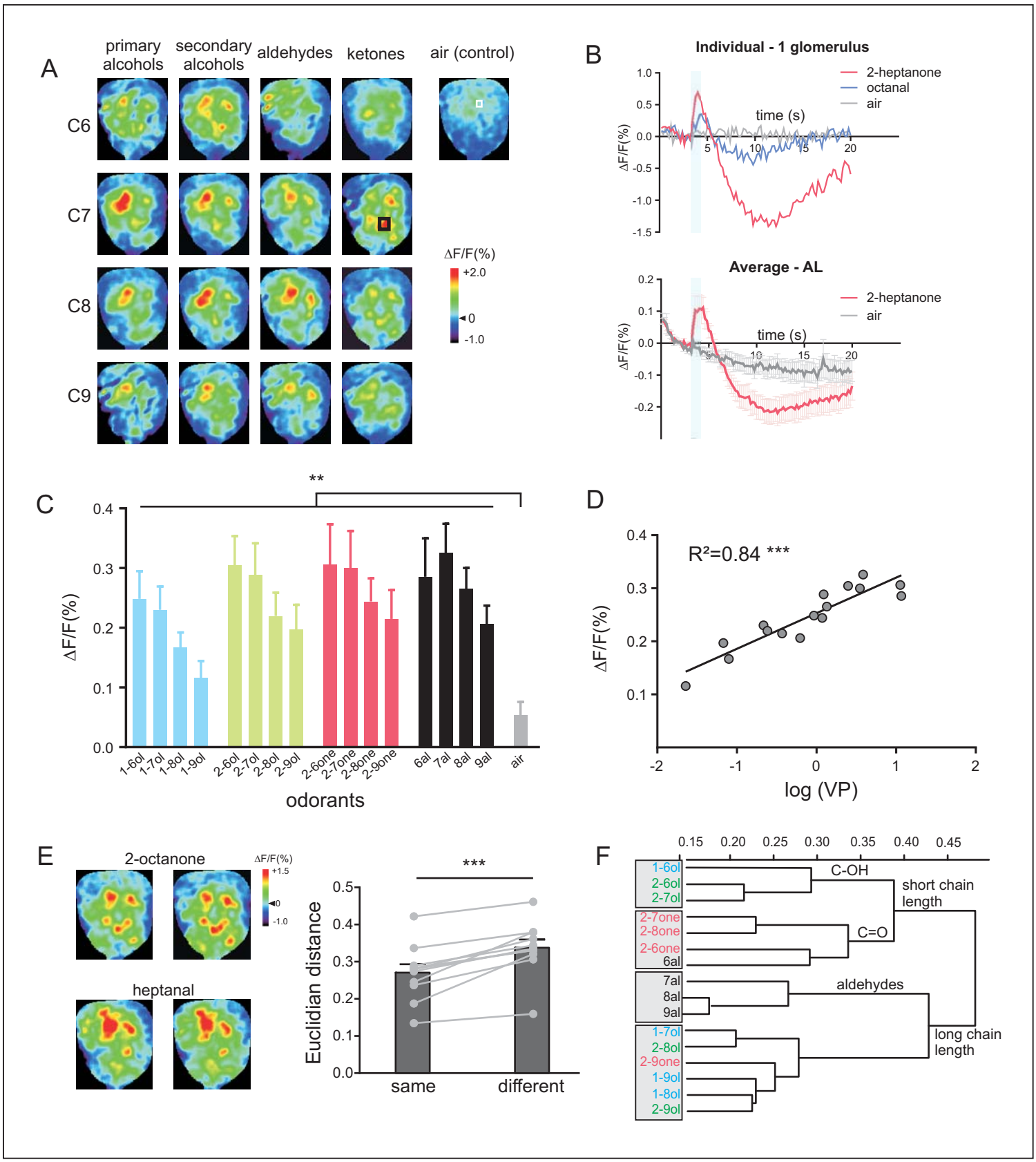
A
primary alcohols
secondary alcohols
aldehydes
ketones
air (control)
C6
C7
C8
C9
ΔF/F(%)
+2.0
0
-1.0
B
Individual - 1 glomerulus
2-heptanone
octanal
air
time (s)
ΔF/F(%)
Average - AL
2-heptanone
air
time (s)
ΔF/F(%)
C
**
ΔF/F(%)
odorants
1-6ol
1-7ol
1-8ol
1-9ol
2-6ol
2-7ol
2-8ol
2-9ol
2-6one
2-7one
2-8one
2-9one
6al
7al
8al
9al
air
D
R²=0.84 ***
ΔF/F(%)
log (VP)
E
2-octanone
heptanal
ΔF/F(%)
+1.5
0
-1.0
***
Euclidian distance
same
different
F
C-OH
short chain length
C=O
aldehydes
long chain length
1-6ol
2-6ol
2-7ol
2-7one
2-8one
2-6one
6al
7al
8al
9al
1-7ol
2-8ol
2-9one
1-9ol
1-8ol
2-9ol

Figure 4

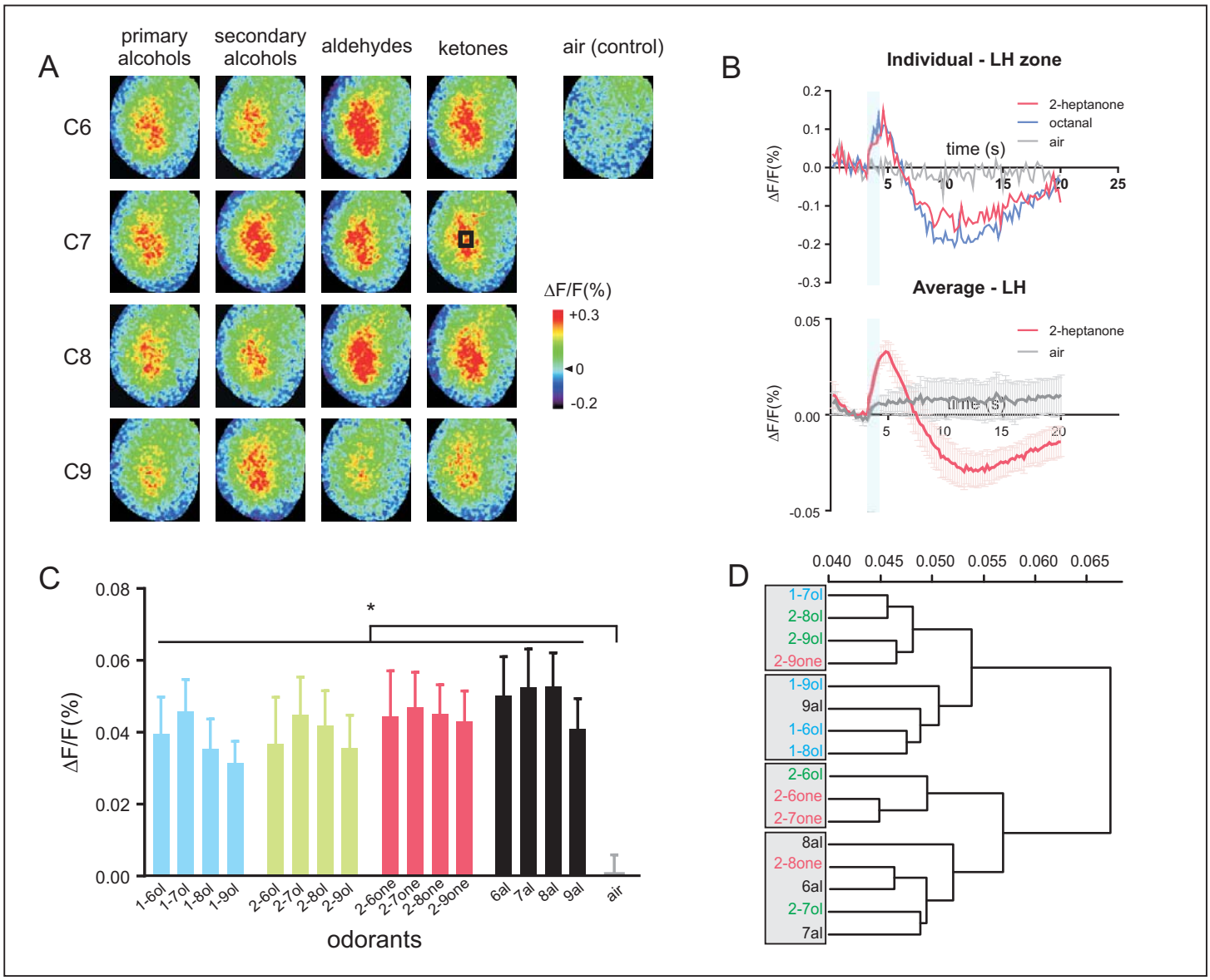
A
primary alcohols
secondary alcohols
aldehydes
ketones
air (control)
C6
C7
C8
C9
ΔF/F(%)
+0.3
0
-0.2
B
Individual - LH zone
2-heptanone
octanal
air
time (s)
ΔF/F(%)
Average - LH
2-heptanone
air
time (s)
ΔF/F(%)
C
ΔF/F(%)
odorants
1-6ol
1-7ol
1-8ol
1-9ol
2-6ol
2-7ol
2-8ol
2-9ol
2-6one
2-7one
2-8one
2-9one
6al
7al
8al
9al
air
D
1-7ol
2-8ol
2-9ol
2-9one
1-9ol
9al
1-6ol
1-8ol
2-6ol
2-6one
2-7one
8al
2-8one
6al
2-7ol
7al

Figure 5

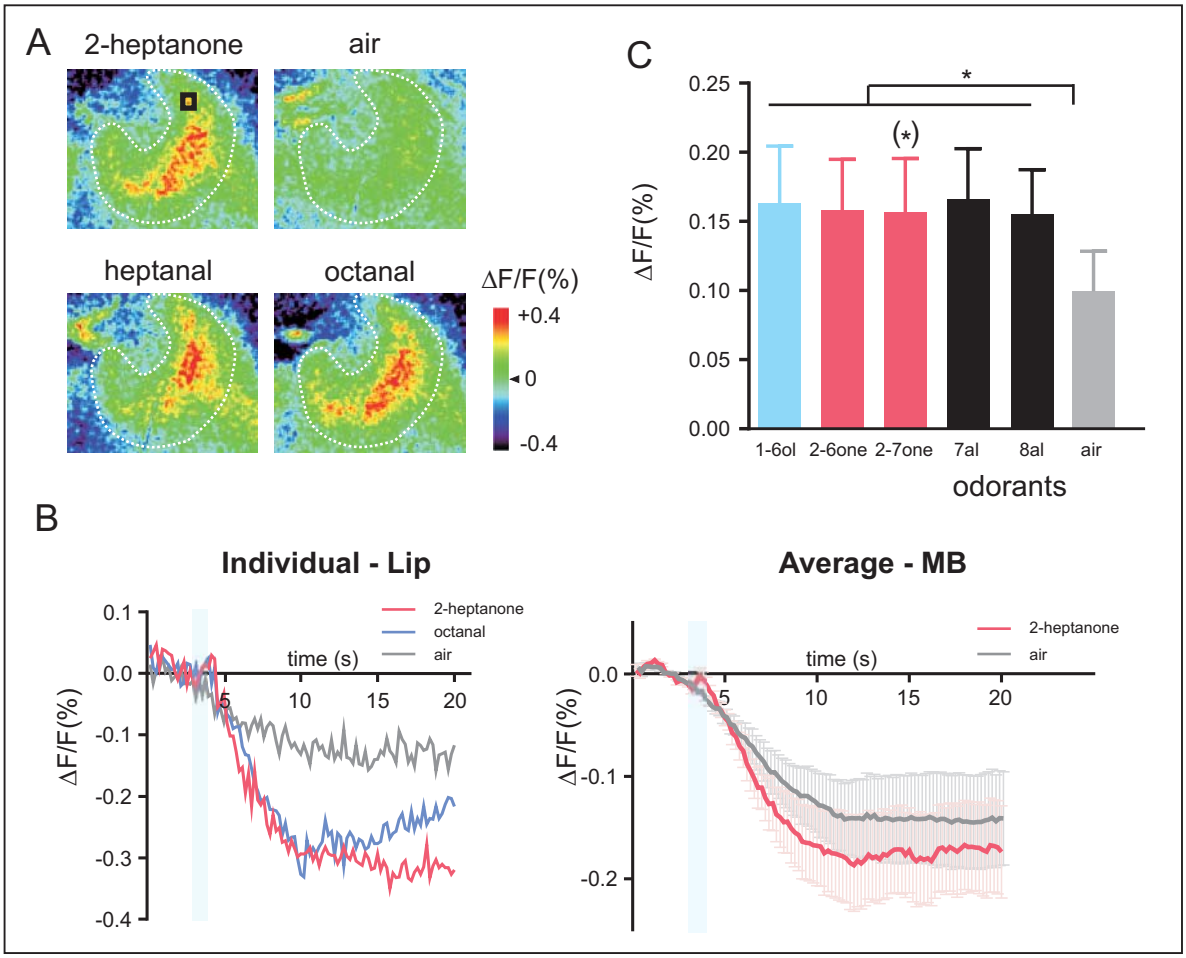
A
2-heptanone
air
heptanal
octanal
ΔF/F(%)
+0.4
0
-0.4
C
0.25
0.20
0.15
0.10
0.05
0.00
ΔF/F(%)
*
(*)
1-6ol
2-6one
2-7one
7al
8al
air
odorants
B
Individual - Lip
Average - MB
2-heptanone
octanal
air
time (s)
0.1
0.0
-0.1
-0.2
-0.3
-0.4
5
10
15
20

Figure 6

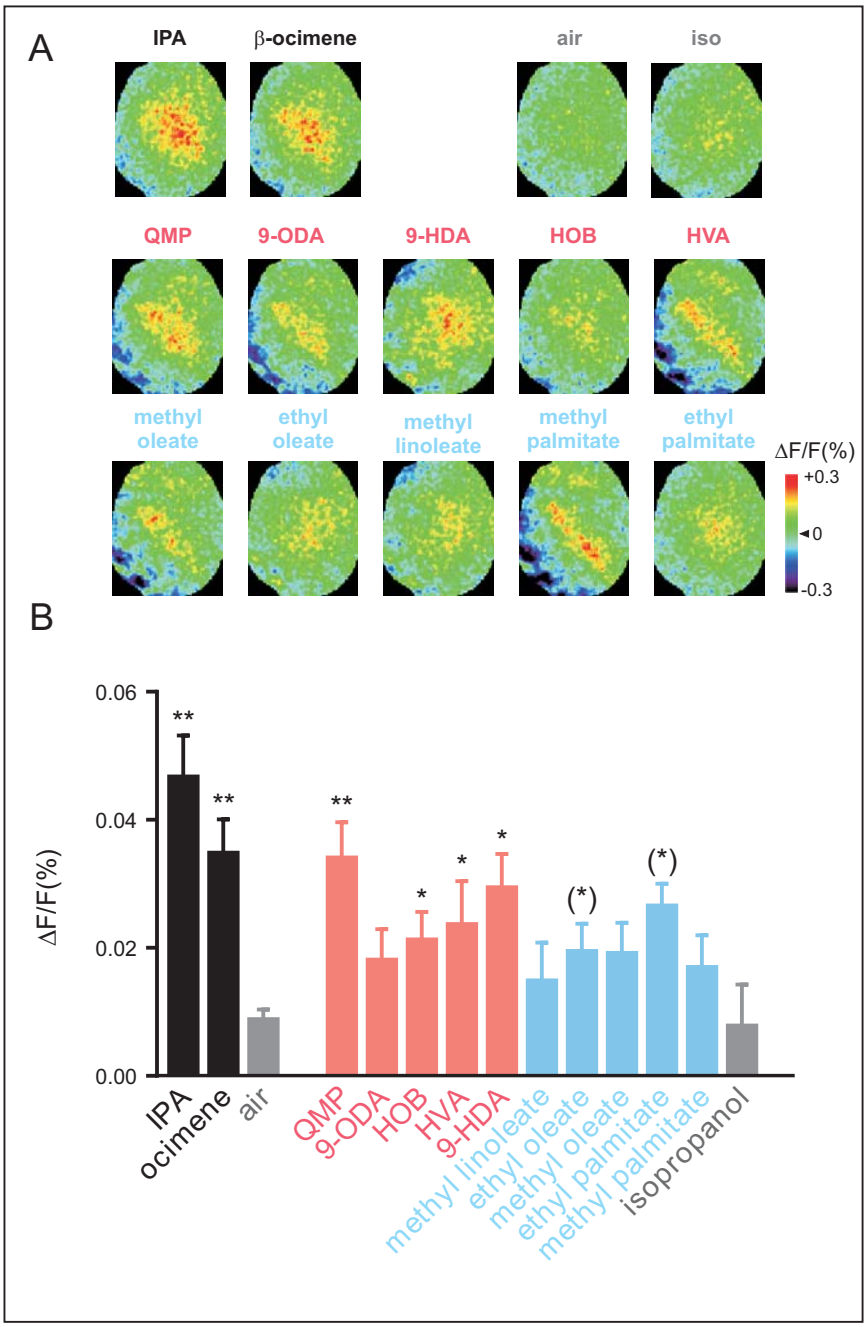
A
IPA
β-ocimene
air
iso
QMP
9-ODA
9-HDA
HOB
HVA
methyl oleate
ethyl oleate
methyl linoleate
methyl palmitate
ethyl palmitate
ΔF/F(%)
+0.3
0
-0.3
B
ΔF/F(%)
0.06
0.04
0.02
0.00
**
**
**
*
*
*
(*)
(*)
IPA
ocimene
air
QMP
9-ODA
HOB
HVA
9-HDA
methyl linoleate
ethyl oleate
methyl oleate
ethyl palmitate
methyl palmitate
isopropanol

S1 Fig.

ACGAGAACCGGGAAGCGTAGTGATAATCTTAATGAAAATCCCCCACGTTCGTGCCTCCTTTGATAGTTTTCACC
CCGGGAAAATGTTTGTGACCCACTTTTCCCACAGAAAACGCTCTAATGCCGTTTTACCTGGGGTGCAAAAAGGT
AGAGTGGGGAAAAAAAAAAAAAAAAGAGGCGGAACCGGAGGAGAGAAGAGAAGAGAGAACCCCGTCTTCT
ACTTGAATACCGTGTCTCGCGCCGTATACGCAAACGTGTACAATATATATAACAATTTTATTGCAAGAATTTCAA
ACAACGCTACGGAGATCAAGGGATCATATAAGAATTTTTATACGTCCTTACAACAGGAAAATTCGTTCCCAAGA
TTCCACGAGTTGTAACGCATGCTGTCTAACCGCACGCATACACACGCACCCCGATACACAATAGAGAAACTCTC
TCTCCTCTCTCTCTCTCTCCCGAAACCGTTTCAAAAATGTACGATCTCCGTAAGATCGTACAAAAGCTCGGGAAT
AAATGCAACGACGAGGAATCACGAATAACTGGGTCGCTGCATTAATTCTTTTATCCAGGCCGACTTATCCGTGG
AGAATGGCGGTCGAGTGGCGAGCAACGAGAAGAATCAACATCATCCATCCGGCACACTCTCTCTATAATTATC
GCGATATCGAAGGAAGGGAAAAAGCGAGGAGTAGAATTTCGAGTTGCAAAGAGATAATATTATATCCCGTTT
CCCTTCCTCCTCCTATTAACTTTCAATCTCATTGCGAACCTCCAGTTTCCTCCAATTTTATATAATATTTTGAAAAG
AGGCGGCTATGCAGAGAATAGAAAAGAAAAAAAAAAGAAAAAGAAGAAATCAGAAGCGCATGCAAACGCGT
TTACCAATGAGCGGGCCGACGTTTCGTCTTCGGTTCGGCCAGCAGGTGGAGCGTGTTTGATGTGAATCGAACA
ACGTCACCCTGTACAAACACCGGGGACCGGGCAGCATATAGGGGCTCGTCCTTTTTTCCCCGTCGTCGTCGTC
GTCGTTAGCTCGCGAGACTGGGTGAGGAGGGGGTGATAAGGAGGACGCAAGCGCGGACCTATCGACCAGCT
AACCCTCCGGGTAACACCCTCGCGATCCTCGGCCGAGGCTCACTGCTTCACCGGCAAACTAGTAGGTAGTACA
CGCACGCGACACAGATTTCAACTTGGATTGTTTAGTTTCTCCTTCCTCACCTCTCTTATTTCATCCTTTCCTTTCGG
ATTACCTTACGTTCAACTGTTATTCCACAAACTCGGCAAGGGAACGCAACATCTCGTTCGAACGCACATCGTCG
AGCGAAGAAGAGATCACGTCGGCGAGACGACGTCCTTTCCGGTAACCGCCGCGTTTACGAGAAAGGGACAGA
CAGAAGGGGGAGAGCGTAGCGGTGTCCACGCCAACGAAAACACCAACGAAGCGGAATTCTGCGGTTTTCGCG
AGGAGGGCGAGGTCGGTGTTAAACCAGCAAGATTACCGGCCGCGGCGGTTGCGCCAAATACTGTGGTACAGC
TACTTCACCCGGCAACATTTCATTCTCCAGCTTTCGACAGTCCTTCACCTCCAATGTTAACTACCTGAAACGGAG
GTTCTCGTCAGGGGATTTGAGCTCGGAGCTCGACGATGAACCAAGCACAGACTCCGGGCTGGCCTCCATG

S2 Fig.

GCaMP-bees

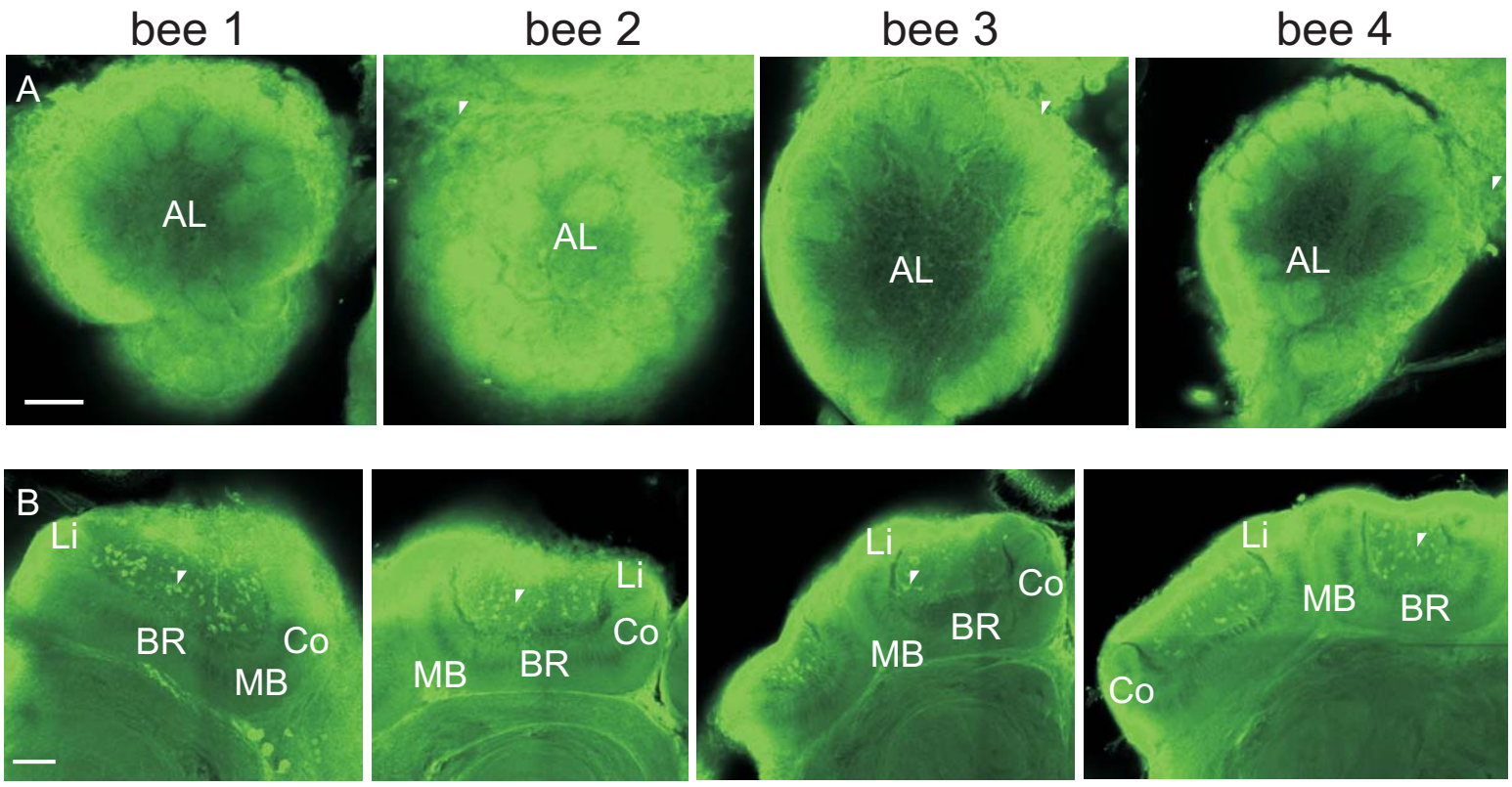

WT bees

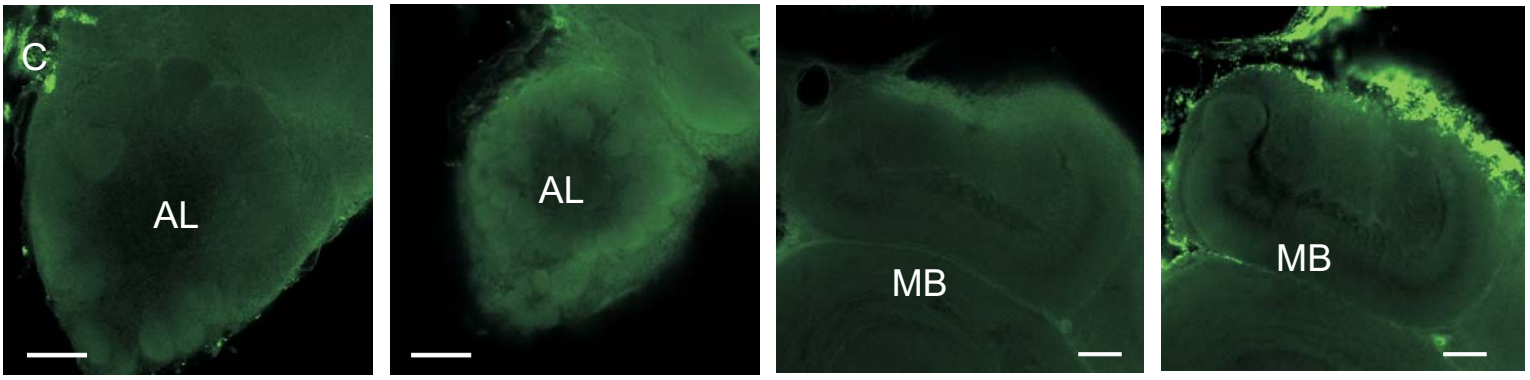

S3 Fig.

A

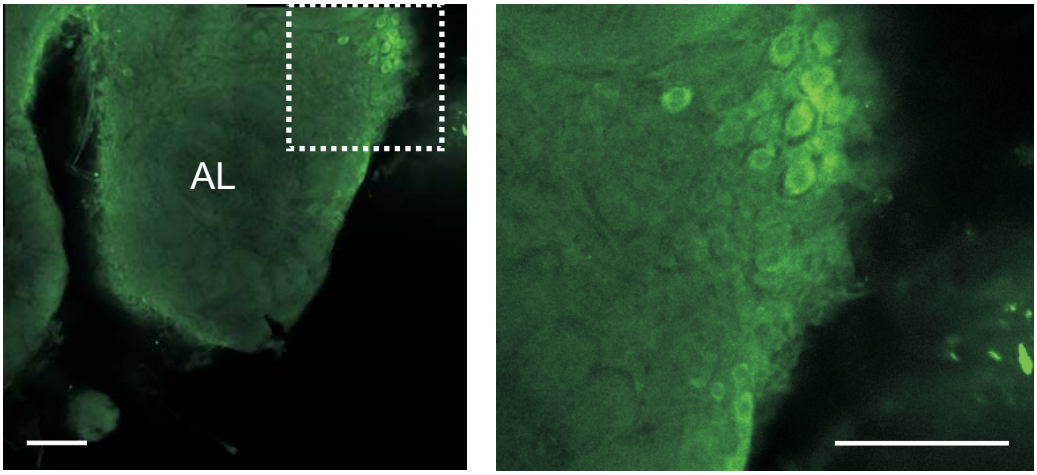

B

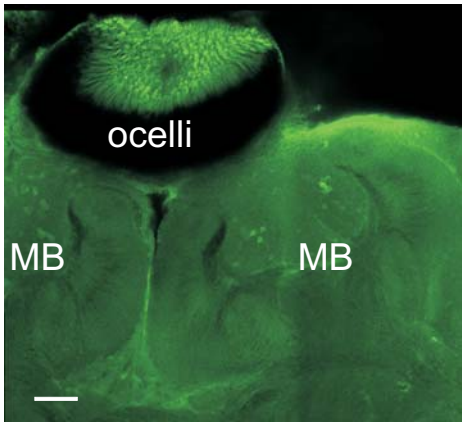

S4 Fig.

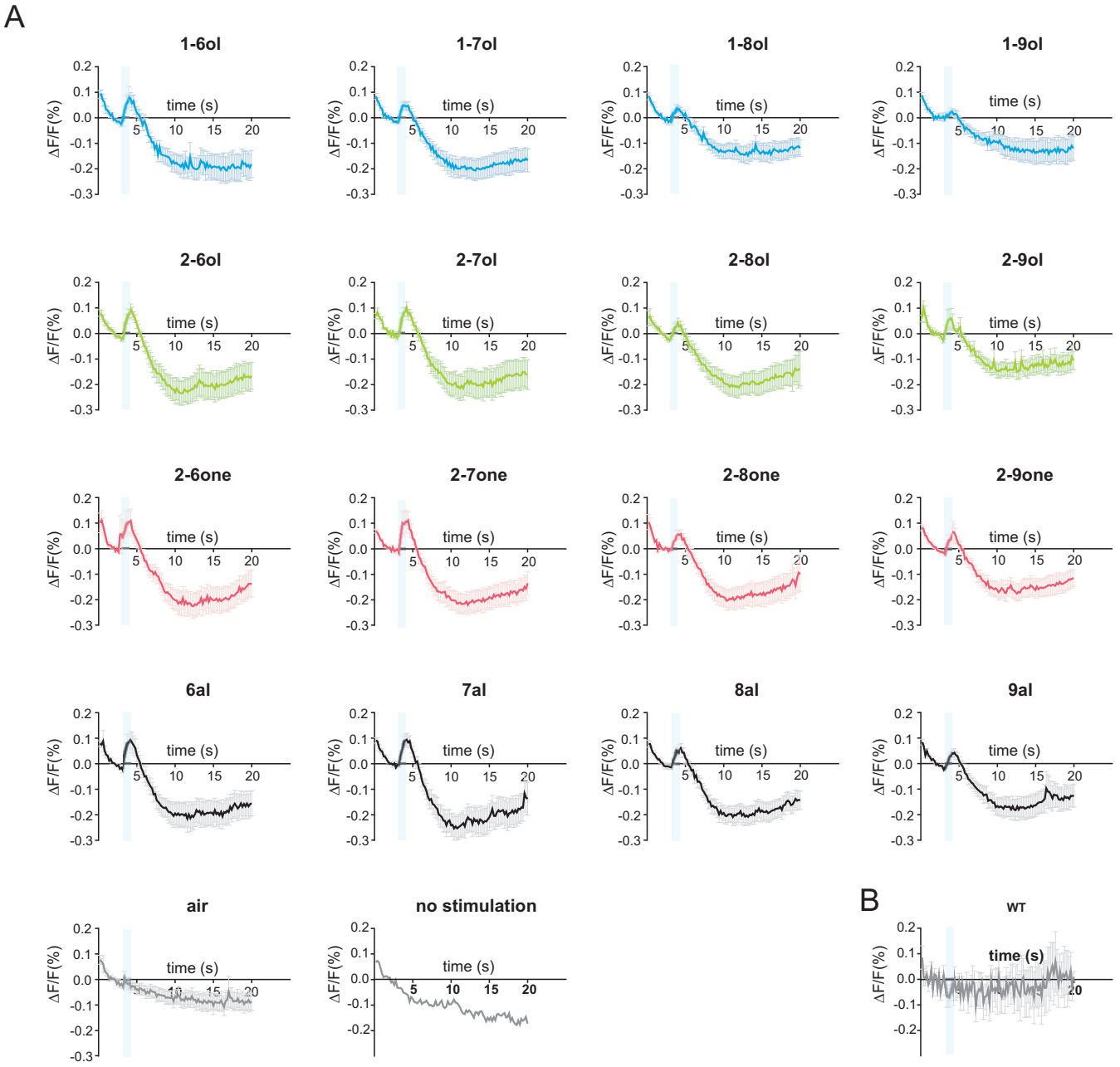
A
1-6ol
1-7ol
1-8ol
1-9ol
2-6ol
2-7ol
2-8ol
2-9ol
2-6one
2-7one
2-8one
2-9one
6al
7al
8al
9al
air
no stimulation
B
WT
ΔF/F(%)
time (s)

S5 Fig.

A

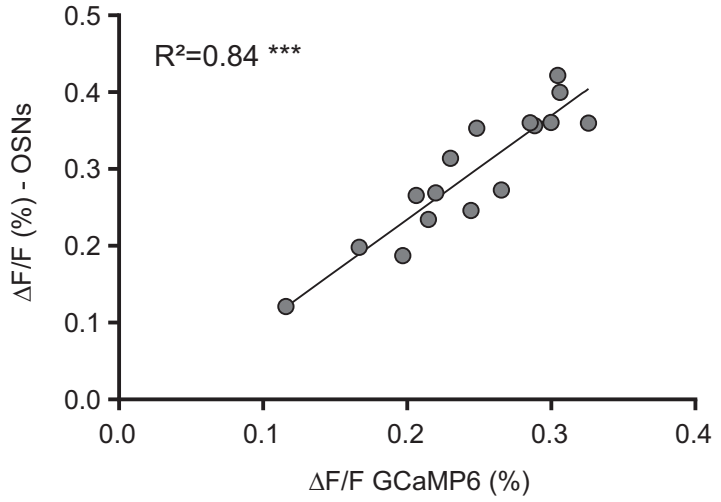
R²=0.84 ***
ΔF/F (%) - OSNs
ΔF/F GCaMP6 (%)
0.0
0.1
0.2
0.3
0.4
0.5

B

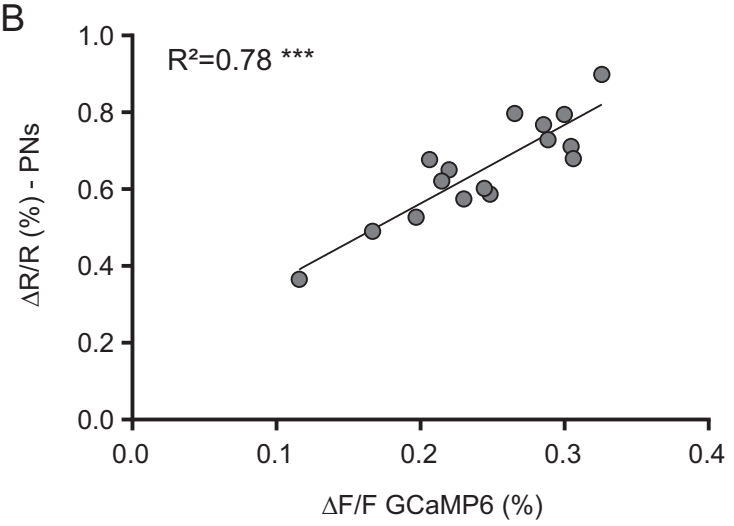
R²=0.78 ***
ΔR/R (%) - PNs
ΔF/F GCaMP6 (%)
0.0
0.2
0.4
0.6
0.8
1.0
0.1
0.3

S6 Fig.

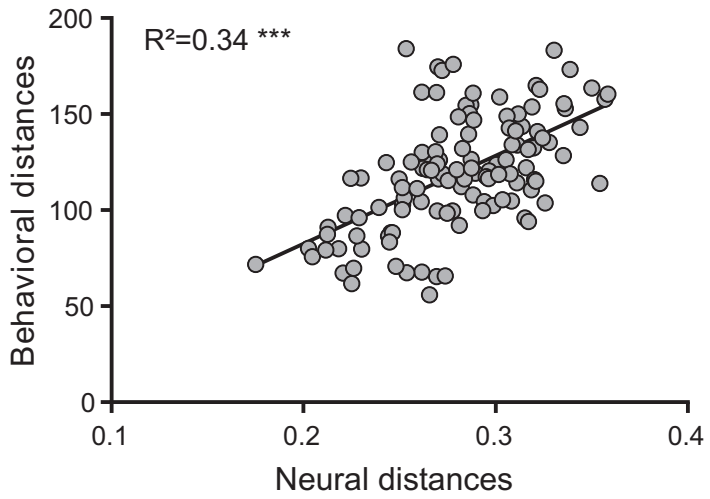
R²=0.34 ***
Behavioral distances
200
150
100
50
0
0.1
0.2
0.3
0.4
Neural distances

S7 Fig.

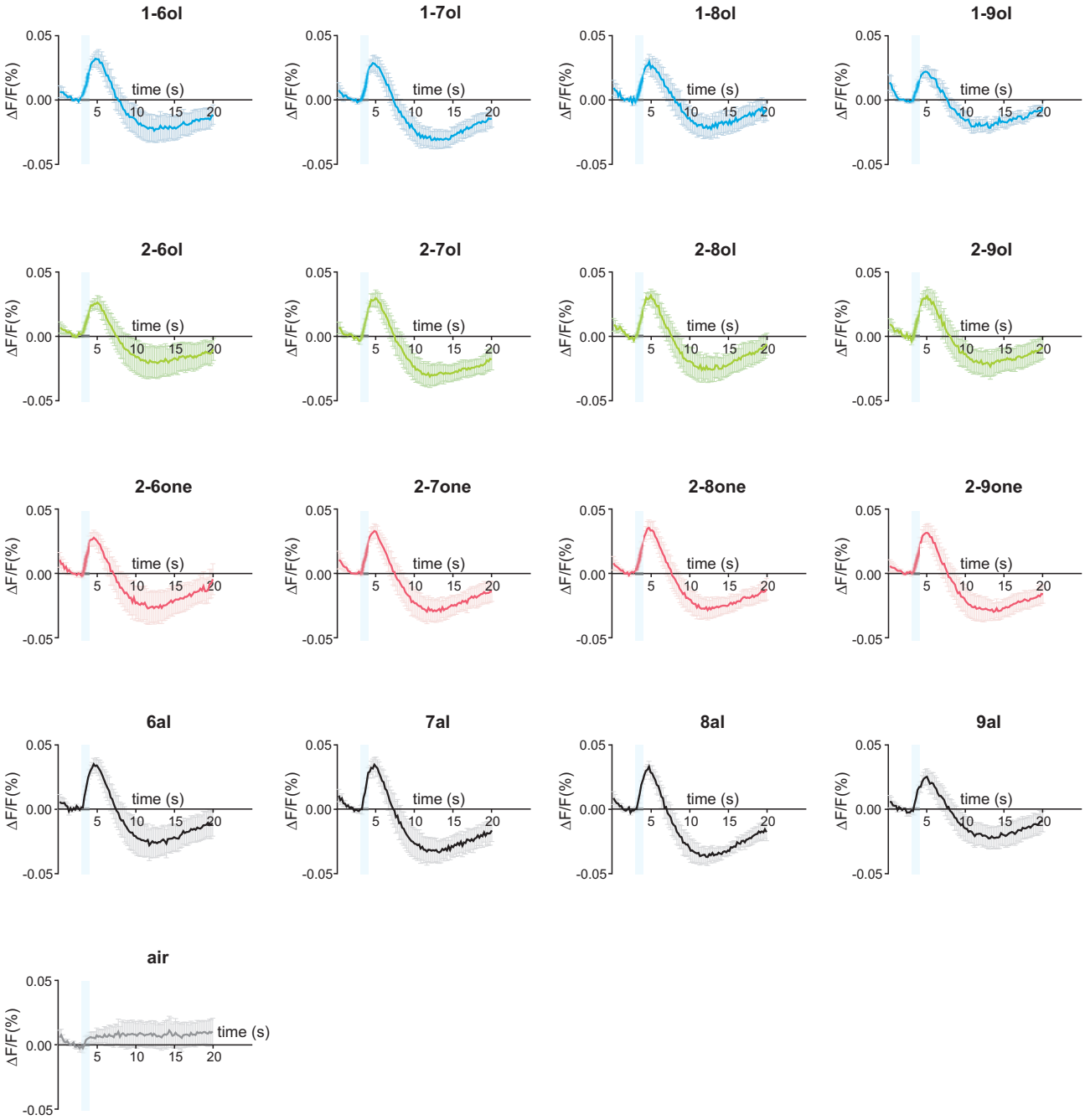
1-6ol
1-7ol
1-8ol
1-9ol
2-6ol
2-7ol
2-8ol
2-9ol
2-6one
2-7one
2-8one
2-9one
6al
7al
8al
9al
air
ΔF/F(%)
time (s)
0.05
0.00
-0.05
5
10
15
20
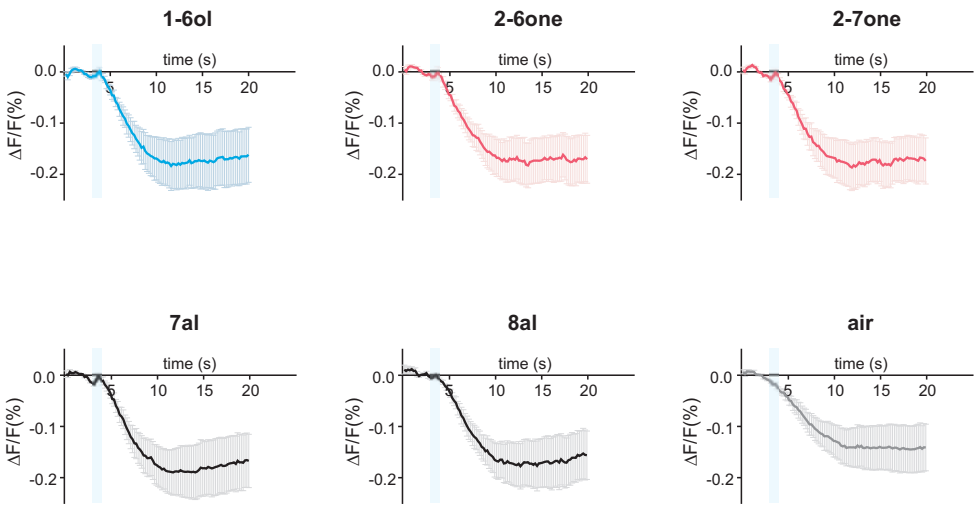
S8 Fig.